Warsaw University of Technology

FACULTY OF PHYSICS

Bachelor's diploma thesis

in the field of study Applied Physics
and specialisation Computer Physics

Analysis of femtoscopic correlations of pion pairs in proton-proton collisions at $\sqrt{s} = 13.6$ TeV in the ALICE experiment at the LHC

thesis number in the Faculty thesis register 105C-ISP-FT/311785/1218334

Alicja Płachta

student record book number: 311785

supervisor:
dr inż. Małgorzata Janik

consultation:
-

WARSAW 2024

Streszczenie

Tytuł pracy: Analiza femtoskopowa korelacji par pionów w zderzeniach proton–proton o energii $\sqrt{s} = 13.6$ TeV w eksperymencie ALICE na LHC.

Femtoskopia to technika analizy używana w celu uzyskania informacji o czasowo-przestrzennych właściwościach źródła emitującego cząstki, takich jak jego rozmiar R. Funkcje korelacyjne ujawniają między innymi efekty korelacji Bosego–Einsteina i oddziaływań kulombowskich. Celem niniejszej pracy inżynierskiej było obliczenie funkcji korelacyjnych dla par pionów $\pi^+\pi^+$, $\pi^-\pi^-$ oraz $\pi^+\pi^-$.

Analizowane dane pochodzą ze zderzeń proton—proton zebranych przez eksperyment ALICE na LHC (Wielkim Zderzaczu Hadronów) w laboratorium CERN, głównie w 2022, ale także w 2018 roku. Głównym narzędziem analizy było O^2, niedawno opracowane w ALICE oprogramowanie zaprojektowane do pracy z nowym formatem danych. Częścią tej pracy było zrozumienie i rozwój jego kodu.

Przeprowadziłam również analizę czystości, wydajności i QA (Quality Assurance – histogramy do oceny jakości danych), aby poprawić selekcję pionów z cząstek wyprodukowanych w zderzeniach.

Przeanalizowałam także symulacje Monte Carlo (PYTHIA 8). Nie uwzględniają one femtoskopowych efektów korelacji Bosego-Einsteina, ale odtwarzają inne efekty i mogą być traktowane jako tło do uzyskania femtoskopowych funkcji korelacji.

Wyniki były podstawą do otrzymania informacji o parametrach źródła. Dla par pionów o identycznym ładunku funkcje mogą być dopasowane eksponencjalnym i gausowskim wzorem Bowlera–Sinyukova co pozwala na otrzymanie rozmiaru źródła R, a także siły korelacji λ. Przeprowadziłam te obliczenia w różnych przedziałach krotności i k_T aby zbadać zależność rozmiaru źródła od tych parametrów. Otrzymane wyniki pokrywają się z oczekiwaniami.

Słowa kluczowe:
ALICE, CERN, piony, femtoskopia, korelacje

{podpis opiekuna naukowego} {podpis dyplomanta}

Abstract

Thesis title: Analysis of femtoscopic correlations of pion pairs in $\sqrt{s} = 13.6$ TeV proton–proton collisions in the ALICE experiment at the LHC.

Femtoscopy is an analysis technique that allows to obtain information about space–time characteristics of the particle–emitting source, such as source size R. Correlation functions reveal, among others, effects of Bose–Einstein correlations and Coulomb interactions. The aim of this thesis was to calculate correlation functions for pairs of pions $\pi^+\pi^+$, $\pi^-\pi^-$ and $\pi^+\pi^-$.

Analysed data comes from proton–proton collisions collected by the ALICE experiment at the Large Hadron Collider at CERN laboratory, mainly from 2022, but also from 2018. The main tool of analysis was O^2, recently developed ALICE framework designed to work with new data format. Part of this work was to understand and develop its code.

I also carried out purity, efficiency and QA (Quality Assurance) analyses to improve the selection of pions from the particles produced in the collisions.

I also analysed Monte Carlo (PYTHIA 8) simulations. They don't include effects of Bose-Einstein correlations but reproduce other effects and can be treated as background to obtain femtoscopic correlation functions. They were the basis to extract information about the source parameters. For identically charged pairs correlation functions can be fitted with Bowler–Sinyukov formula, both exponential and Gaussian, and source size R, as well as correlation strength λ, can be found. I have carried out the calculations in different intervals of multiplicity and pair transverse momentum k_T in order to examine dependance of source size on these variables. Obtained results are in line with expectations.

Keywords
ALICE, CERN, pions, femtoscopy, correlations

{supervisor's signature} {diplomant's signature}

Oświadczenie o samodzielności wykonania pracy

Politechnika Warszawska

Alicja Płachta
311785
Fizyka Techniczna

Oświadczenie

Świadomy/-a odpowiedzialności karnej za składanie fałszywych zeznań oświadczam, że niniejsza praca dyplomowa została napisana przeze mnie samodzielnie, pod opieką kierującego pracą dyplomową.

Jednocześnie oświadczam, że:

- niniejsza praca dyplomowa nie narusza praw autorskich w rozumieniu ustawy z dnia 4 lutego 1994 roku o prawie autorskim i prawach pokrewnych (Dz.U. z 2006 r. Nr 90, poz. 631 z późn. zm.) oraz dóbr osobistych chronionych prawem cywilnym,
- niniejsza praca dyplomowa nie zawiera danych i informacji, które uzyskałem/-am w sposób niedozwolony,
- niniejsza praca dyplomowa nie była wcześniej podstawą żadnej innej urzędowej procedury związanej z nadawaniem dyplomów lub tytułów zawodowych,
- wszystkie informacje umieszczone w niniejszej pracy, uzyskane ze źródeł pisanych i elektronicznych, zostały udokumentowane w wykazie literatury odpowiednimi odnośnikami,
- znam regulacje prawne Politechniki Warszawskiej w sprawie zarządzania prawami autorskimi i prawami pokrewnymi, prawami własności przemysłowej oraz zasadami komercjalizacji.

Warszawa, dnia {podpis dyplomanta}

Oświadczenie o udzieleniu Uczelni licencji do pracy

Politechnika Warszawska

Alicja Płachta
311785
Fizyka Techniczna

Oświadczenie studenta w przedmiocie udzielenia licencji Politechnice Warszawskiej

Oświadczam, że jako autor/współautor[1] pracy dyplomowej pt. *"Analysis of femtoscopic correlations of pion pairs in proton-proton collisions at* $\sqrt{s} = 13.6$ *TeV in the ALICE experiment at the LHC"* udzielam/nie udzielam[1] Politechnice Warszawskiej nieodpłatnej licencji na niewyłączne, nieograniczone w czasie, umieszczenie pracy dyplomowej w elektronicznych bazach danych oraz udostępnianie pracy dyplomowej w zamkniętym systemie bibliotecznym Politechniki Warszawskiej osobom zainteresowanym.

Licencja na udostępnienie pracy dyplomowej nie obejmuje wyrażenia zgody na wykorzystywanie pracy dyplomowej na żadnym innym polu eksploatacji, w szczególności kopiowania pracy dyplomowej w całości lub w części, utrwalania w innej formie czy zwielokrotniania.

Warszawa, dnia {podpis dyplomanta}

[1] Niepotrzebne skreślić.

Contents

Chapter 1

Introduction

1.1. Particle physics

For thousands of years people have tried to answer questions about how our universe works. Humanity's persistence in trying to find the answers and developing scientific methods has contributed to the overall advancement of technology, medicine and all aspects of our daily lives. One of the greatest unknown was always the inner structure of matter. Philosophers and physicists came up with many theories, from the Greek idea of the atom through plum pudding model and electron discovery by Thompson. Among the major breakthroughs are Rutherford's experiment discovering nucleus and Bohr's work, as well as quantum theories of atomic structure.

In the nineteenth century the current most important theory in particle physics was developed: the Standard Model. It elegantly puts elementary particles in categories of fermions (quarks and leptons) and bosons according to their properties. It describes most fundamental particles and the forces between them. High-energy experiments have been established in order to find experimental proof of worked out theories. New discoveries were being made using collisions of ions and hadrons (particles composed of quarks) at large energies.

From the point of view of this thesis an important finding in the history of particle physics is the discovery of pions. These mesons were postulated by Yukawa already in the 1930s in his description of strong nuclear force [1]. Experimentally, their existence was confirmed more than ten years later, in 1947, after Latte, Muirhead, Occhialini and Powel observed their presence in cosmic rays thanks to nuclear emulsions [1]. Pions are mesons, particles made up of quark and antiquark, in this case up u (antiquark up $\bar{u}$) and down d (antiquark down $\bar{d}$). There are three types of pions, which differ in charge due to their structure [2]:

- π^0 which is not the subject of this thesis,
- $\pi^+ = u\bar{d}$,
- $\pi^- = \bar{u}d$.

This thesis analyses data from proton–proton collisions. Study of these events is an intriguing subject and can provide interesting insights into high-energy physics. Pions are the majority of particles formed in a collision, so pion analysis is not troublesome when it comes to statistics but it is still beneficial to study p–p collisions at higher energies to obtain larger multiplicities of created particles.

There are many ways of studying collisions and learning about particles and interactions. One of these methods is femtoscopy, which is described in more detail in the upcoming section.

1.2. Femtoscopy

Femtoscopy is a technique allowing us to obtain information about the space-time characteristics of the particle-emitting source by measuring correlations between particles. Femtoscopic correlation function is given by the equation [3]:

$$C(k^*) = \int S\left(\vec{r^*}\right)\left|\Psi_{-\vec{k^*}}\left(\vec{r^*}\right)\right| d^3\vec{r^*}. \tag{1.1}$$

It is a function of k^*, observable related to particles momentums by $k^* = \frac{1}{2}(p_1 - p_2)$. In equation 1.1 $\Psi_{-\vec{k^*}}\left(\vec{r^*}\right)$ is two particle wave function. It can usually be analytically found for each analysed particle pair.

$S(r)$ in equation 1.1 is the source function related to the source size. The goal of femtoscopic analysis is to get information about its parameters. In order to achieve that, the correlation function must be determined. Experimentally correlation functions are produced by dividing k^* histograms for particles from the same and mixed events ($N_{SE}(k^*)$ and $N_{ME}(k^*)$ respectively) and then normalizing them, so they tend to one [4]:

$$C(k^*) = \mathcal{N}\frac{N_{SE}(k^*)}{N_{ME}(k^*)}. \tag{1.2}$$

It usually is done for different multiplicitiy intervals as well as transverse mass m_T or transverse momentum k_T. Those are values related to transverse momenta of both particles [5]:

$$k_T = \frac{\left|p_{T_1} + p_{T_2}\right|}{2}, \tag{1.3}$$

$$m_T = \sqrt{k_T^2 + m^2}. \tag{1.4}$$

Results obtained with equation 1.2 include effects of non-femtoscopic correlations. There are two approaches to removal of this background. One of them is producing "correlation functions" from Monte Carlo data. Some models used for this type of simulations do not include femtoscopic effects of Bose–Einstein correlations and the results of such an analysis can be treated as background. In this thesis I used this method. Another way is to apply a transverse sphericity cut on collisions during data analysis. The sphericity gives us information about how close the shape of the source is to the ideal sphere ($S_T = 1$). For higher sphericities the results present mainly femtoscopic effects. Mathematically transverse sphericity S_T is defined as [5]

$$S_T = \frac{2\min(\lambda_1,\lambda_2)}{\lambda_1 + \lambda_2} = \frac{1}{\sum_i p_T^i}\sum_i \frac{1}{p_T^i}\begin{bmatrix}(p_x^i)^2 & p_x^i p_y^i \\ p_x^i p_y^i & (p_y^i)^2\end{bmatrix}. \tag{1.5}$$

The parameters λ are eigenvalues of this transverse momentum matrix for the i-th particle [5].

By fitting calculated functions the source size can be found. For fitting same charged pions functions I used two different Bowler–Sinyukov formulas [5]. One is assuming Gaussian shape of the source:

$$C(k^*) = 1 - \lambda + \lambda \cdot K(k^*) \cdot \left[1 + \exp\left(-4R^2 \cdot k^{*2}\right)\right], \tag{1.6}$$

end the second exponential:

$$C(k^*) = 1 - \lambda + \lambda \cdot K(k^*) \cdot \left[1 + \exp\left(-2R \cdot k^*\right)\right]. \tag{1.7}$$

In both equation 1.6 and 1.7 λ is correlation strength and R is the source size. $K(k*)$ is a Coulomb function for a given $k*$.

Although out of scope of this work, it is worth mentioning that multi–dimentional correlation functions can be also studied and provide additional information about source.

Femtoscopy is versitile analysis and can help to deepen our knowledge about interactions beetween particles and properties of collisions. For pions correlation functions shape shows effects of Bose-Einstein correlations and Coulomb interactions. In $\pi^+\pi^-$ function peaks related to resonance decays can be seen. This analysis can also reveal effects of mini jets and other non-femtoscopic corellations.

In this thesis pion correlation functions were produced and analysed.

Chapter 2

Data collection

2.1. CERN

The European Organization for Nuclear Research, more widely known as CERN, is an established in 1954 science facility, located on the Swiss and French border near Geneva [6]. Currently it associates 23 countries and over 17 500 people [7]. As CERN states on its official website part of its mission is uniting scientist from all around the world and providing tools for research in fundamental physics [8]. The achievements of CERN have contributed tremendously to modern physics, as well as technology. Among many of them are Higgs boson discovery [9], invention of The World Wide Web or solutions used in healthcare, for instance in PET (Positron Emission Tomography) scanners [10]. Thanks to CERN policy its work results are avaiable to the public enabling others to benefit from these achievements.

There are many experiments related to CERN Laboratory covering a broad range of science. Other than ALICE, there are two experiments worth mentioning, that Faculty of Physics at Warsaw University of Technology is also involved in: AEgIS (Antihydrogen Experiment: Gravity, Interferometry, Spectroscopy) aiming to learn about gravity impact on antimatter or NA61/SHINE (the SPS Heavy Ion and Neutrino Experiment) studying hadrons [11].

The CERN biggest accelerator is LHC - The Large Hadron Collider [12]. It is 27 kilometer long particle accelerator that started its operation in 2008 (replacing former device The Large Electron-Positron Collider). It uses superconducting magnets and electric field to accelerate heavy ions and protons to almost light speed and gives ability to collide them at high energies. LHC is an incredile engineer achievement, as it uses high vacuum and is able to cool its magnets to 1,9 K [12].

The particles collide at four points when big experiments can collect data from them. There are:

- ALICE – A Large Ion Collider Experiment [13],
- ATLAS – A Toroidal LHC Apparatus [14],
- CMS – The Compact Muon Solenoid [15],
- LHCb – The Large Hadron Collider beauty [16].

The period of LHC running is called Run. It is followed by Long Shutdown during which the experiments and LHC can make adjustments and changes in their detectors and operations. Currently

Run 3 is ongoing. It enables collisions at energy up to 13.6 TeV. ALICE Experiment had underwent important changes before that, as explained in the next section.

2.2. ALICE

ALICE (A Large Ion Collider Experiment) is a detector at the LHC dedicated to collecting data from heavy–ion collisions, but it also collects data from proton and p–nuclei collisions, or, as in the case of data analysed in this thesis, high energy proton–proton collisions. ALICE Collaboration came to life in 1993 [17] and according to its official website currently assiociates almost two thousand people from 169 institutes from 40 countries [18], among them Faculty of Physics of Warsaw University of Technology.

ALICE detector consists of eighteen different detectors. ALICE current structure is shown in figure 2.1. One of the most important detectors are ITS (The Inner Tracking System), TPC (Time-Projection Chamber) and TOF (Time of Flight Detector), that play a vital role in tracks reconstruction and particle identification. I used signals from them in my work.

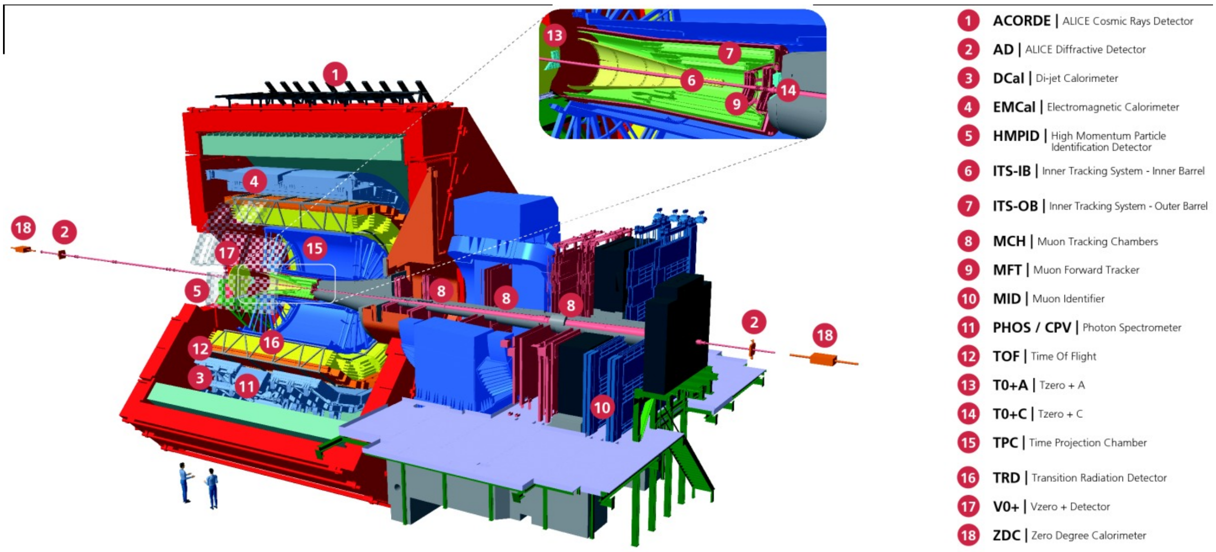

(Source: CERN Document Server. ALICE Schematics as during RUN3 (after upgrade), Photograph: Tauro, Arturo, ALICE-PHO-SKE-2017-001-5.)

Figure 2.1: ALICE Schematics during RUN3.

Before Run 3, during LHC Long Shutdown 2, ALICE experiment underwent many changes, in order to maximalise data taking efficiency and quality. Among those modifications are upgrades of detectors: ITS (Inner Tracking System), TPC (Time Projection Chamber), and TOF (Time of Flight). These are descibed in the next sections. Important change was a switch to continuous readout rate – upgrades of detectors, mainly TPC, forced redesign of readout infrastructure. This system has numerous steps: data goes to First Level Processors and is grouped into time frames, then the farm of Event Processing Nodes performs online collisions reconstruction and the output is stored for offline reconstruction and analysis using new framework O^2 [19].

2.2.1. ITS

ITS (Inner Tracking System) is the detector closest to the colliding beams. It enables to reconstruct the collision point i.e. the primary vertex, as well as secondary vertices from particles decays [13]. It also plays a role in particles tracking. Detectors used in ITS are semiconductors detectors.

During Long Shutdown 2 ITS was entirely changed. Before, it consisted of two layers of Silicon Pixel Detectors, two layers of Silicion Drift Detectors, and two double sided Silicon micro-Strip Detectors. The detailed technical describtion of these devices can be found in ALICE Collaboration article [13]. After upgrade additional detector layer was added and pixel sensors were upgraded. The first layer is now closer to the collision point – 22.4 mm comparing to 39 mm before [19]. Detectors in use are now ALPIDE monolithic active pixel sensors. ITS2, as the upgraded version is called, can fulfill its tasks with better resolution and with much larger readout rate (up to 50 kHz, comparing with 1 kHz before [19]) allowing overall better performance of ALICE experiment.

2.2.2. TPC

TPC (Time Projection Chamber) is the most important ALICE detector. It is vital in particle identification, tracking charged particles, momentum measurements as well as localizing vertices [13]. It covers full azimuth, large transverse momentum and pseudorapidity η ranges [13] (pseudorapidity is a value related to the angle to the beam (z axis) θ of the created particle by equation $\eta = -\ln\left[\tan\left(\theta/2\right)\right]$ [20]). TPC detector measures the average energy loss dE/dx (described by Bethe-Bloch formula [21]) that is characteristic for each particle species and allows their identification.

It is a gas detector. It uses 90 m^3 of $Ne/CO_2/N_2$ in proportions of 90/10/5 [13]. Charged particles ionise this gas and free electrons travel through the chamber thanks to the electric field. This makes their detection possible.

The limitation of TPC was the drift time (around 100 μs). At higher collision rates tracks from different collisions would pile up and not all events could be registered. During Long Shutdown 2 TPC underwent many changes with the goal of implementing continous readout which makes collecting more data possible. Multiwire Proportional Chambers (MWPCs) were replaced by stacks of four Gas Electrons Multipliers [19].

2.2.3. TOF

The TOF (Time of Flight) together with previously mentioned detectors is important in particle identification of pions, kaons, and protons [13]. It allows to measure time of flight for each track from which its velocity can be determinated. Gaseous detectors that TOF is using are Multi-gap

Resistive-Plate Chambers (MRPC) [13]. As others detectors, it also needed to undergo upgrades of its readout electronics to implement continous readout.

2.3. ALICE Control Centre

Operation of ALICE experiment is monitored and controlled from ALICE Run Control Centre. During the data taking period at least four people (shifters) are present in ARC and take care of data taking, its quality and detectors operation [22]. Those role can be performed by each experiment participant after relevant training. Shifters roles are:

- SL (Shift Leader) – person responsible for actions taken in control room,
- ECS (Experiment Control System) shifter – person controling ECS, starting data taking with proper settings and detectors as well as monitoring readout,
- DCS (Detector Control System) shifter – person responsible for detectors operations and reacting in case of their errors,
- QC (Quality Control) shifter – person monitoring data quality, allowing to spot problems with experiment operation.

Other roles that are important to mention are Run Coordination and Run Manager supervising ALICE operation as well as detectors experts that know the details of its structure.

2.4. Used data

In this thesis data from proton–proton collisions collected by the ALICE experiment in 2018 during Run 2 of LHC operation and in 2022 during Run 3 was used. ALICE data is organised in datasets based on period of taking and collisions parameters (like interaction rate). I conducted my analysis on Run 2 data converted to O^2 format, Run 3 data, and Monte Carlo (MC) simulations anchored to Run 3 data. MC simulations are run using experiment computing system based on configurations from real data taking and intend to reproduce events from dataset to which they are anchored. They use PYTHIA 8 Monte Carlo generator dedicated for high–energy physics. Monte Carlo datasets consist information about all particles created in an event that can be compared to information about detected tracks. The datasets I used are:

- Run 2:
  - **LHC18l**: p–p collisions at $\sqrt{s}$ = 13 TeV. Runs 289240, 289241, 289242, 289243, 289247, 289249, 289253, 289254, 289275, 289276, 289277, 289278, 289280, 289281, 289300, 289303, 289306, 289308, 289309, 289330, 289331, 289353, 289354, 289355, 289356, 289363, 289365, 289366, 289367, 289368, 289369, 289370, 289373, 289374, 289426, 289444, 289462, 289463, 289465, 289466, 289468, 289493, 289494, 289521, 289547, 289574, 289576, 289577, 289582, 289625, 289632, 289634, 289657, 289658, 289659, 289660, 289664, 289666, 289721, 289723, 289724, 289729, 289731, 289732, 289757, 289775, 289808, 289811, 289814, 289815, 289816,

289817, 289818, 289830, 289849, 289852, 289854, 289855, 289856, 289857, 289879, 289880, 289884, 289928, 289931, 289935, 289940, 289941, 289943, 289965, 289966, 289971.

- Run 3:
  - **LHC22f_pass4** (part of LHC22_pass4_lowIR): p–p collisions at $\sqrt{s}$ = 13.6 TeV. Runs 520259, 520294, 520471, 520472, 520473.
  - **LHC22o_pass4_minBias_small**: p–p collisions at $\sqrt{s}$ = 13.6 TeV. Run 526641.
- Run 3 MC:
  - **LHC23d1k**: PYTHIA 8 model, p–p collisions at $\sqrt{s}$ = 13.6 TeV, anchored to LHC22f apass4.
  - **LHC23f4b2**: PYTHIA 8 model, p–p collisions at $\sqrt{s}$ = 13.6 TeV, anchored to LHC22o apass4.

Although LHC22f_pass4 has smaller statistics than LHC22o_pass4_minBias_small, Monte Carlo dataset anchored to it LHC23d1k has larger statistics than LHC23f4b2 allowing analysis using MC simulations for background removal. Futhermore, conclusions from the analysis of LHC22o_pass4_minBias_small are similar to those from LHC22f_pass4. For this reason results shown in the rest of this thesis come mostly from LHC22f_pass4 and results for LHC22o_pass4_minBias_small are shown in appendix A. Exact statistics after applied cuts are presented in table 2.1. Process of selection and choice of cuts is presented in section 3.3.

Table 2.1: Statistics in each used dataset after applying cuts.

Dataset	**Events**	π^+	π^-
LHC18l	$2.68 \cdot 10^8$	$1.67 \cdot 10^9$	$1.67 \cdot 10^9$
LHC22f_pass4	$6.52 \cdot 10^7$	$1.84 \cdot 10^8$	$1.83 \cdot 10^8$
LHC22o_pass4_minBias_small	$3.08 \cdot 10^9$	$7.84 \cdot 10^9$	$7.85 \cdot 10^9$
LHC23d1k	$7.08 \cdot 10^7$	$2.26 \cdot 10^8$	$2.26 \cdot 10^8$
LHC23f4b2	$1.40 \cdot 10^7$	$4.10 \cdot 10^7$	$4.10 \cdot 10^7$

Chapter 3

Data analysis

3.1. O2

O^2 (The Online-Offline) [23] is an analysis framework developed during Long Shutdown 2 to deal with Run 3 data. Run 2 can be converted and also be analysed with it. O^2 is based on C++17 and it supports use of ROOT objects and Apache Arrow columnar data format offering efficient options of accesing needed data. Analysis framework is developed by its users and is still constantly changing. The code is public and can be found on Github alongside the documentation [24, 25].

To carry out my work I needed to understand and develop code in *O2Physics* (part of O^2 for analysis). I started to work in FemtoWorld - part of *O2Physics* that was developed in the previous year by the ALICE group at Warsaw University of Technology. Later, FemtoUniverse was created to improve and simplify cooperation between groups. It uses better programming practices and is more efficient comparing to the previous code. Thanks to many tutorials I attended as well as existing code in this framework I was able to understand it and add my contributions. I mainly worked on files:

- *O2Physics/PWGCF/FemtoUniverse/Tasks/femtoUniversePairTaskTrackTrackMultKtExtended.cxx* – main task for creating k^* histograms (used as numerators and denominators of the $\pi\pi$ correlation functions),
- *O2Physics/PWGCF/FemtoUniverse/Core/FemtoUniversePairWithCentMultKt.h* – for creating k^* histograms in different ranges of multiplicity and transverse momentum,
- *O2Physics/PWGCF/FemtoWorld/Tasks/femtoWorldEfficiencyTask.cxx* – for analysis of purity and efficiency, as well as quality of data and selection.

Another important file worth mentioning is *femtoUniverseProducerTask.cxx* which performs the initial event and track selection and creates data arrays used by the other tasks in the FemtoUniverse. When running an analysis firstly producer must be run together with needed helper tasks available in O^2. They return output data file that normal analysis task can be run on.

k^* histograms selected for pions from same and mixed events are calculated using task in *femtoUniversePairTaskTrackTrackMultKtExtended.cxx*. The results are presented in k^* histograms for full data, as well as for different multiplicity N and k_T ranges. For creating pairs of identical particles from the same event I used the so-called strictly upper index policy for which combinations exclude repeated indexes, for instance (1,2) and (2,1), as well as (1,1) or (2,2) and so on [25].

For non-identical particles or particles from different events I used so-called full index policy for which combinations include repeated indexes [25]. When mixing events each event is mixed with five others that have similar values of multiplicity (within 4) and z coordinate of primary vertex (within 2 cm).

In the next step I used ROOT macros to process the output. The result of the k^* division has to be normalised so that its flat part tends to one. I did this by integrating over a chosen k^* range for which the function is flat, dividing this value by the range width and eventually scaling the correlation function. For the correlation functions for the full range of k_T (including those for different mulitplicities ranges) I chose this range as $k^* \in [0.5, 0.7]$. For functions for different k_T ranges I used the range $k^* \in [0.4, 0.5]$ as over this limit functions were behaving differently for some ranges, or the statistics decreased.

3.2. Hyperloop and Grid

Hyperloop is a web tool enabling physicists to run the task developed in *O2Physics* on the Grid – the network combining around 1.4 million computer cores [26] providing recources to conduct analysis on large amount of data. The Hyperloop system is based on wagons that are linked to tasks in *O2Physics*. They can be configured and composed in trains that are run for a chosen dataset via web page that also provides easy access to the results. All results presented in this thesis were obtained using Hyperloop.

3.3. Event and track selection

Cuts are applied to events in order to select good quality data. For instance cut for z coordinate (along the beam) of primary vertex is applied as for collisions too far away from the middle of ALICE detector all created particles cannot be properly registered. Tracks cuts have to be applied to select good data, but also to select pions for analysis from among many particles of different species. In my analysis I decided to apply following cuts:

- Event cuts:
  - build–in *O2Physics* filters (called sel7() for Run 2 and sel8() for Run 3) that select good quality events, correct for pileup that occurs when detectors collect data from more than one event at the same time (especially present in data with high interaction rate, i.e higher frequency of collisions), etc.
  - $-10 < vtx_z < 10$ cm.
- Tracks cuts:
  - $0.14 < p_T < 1.5$ GeV/c,
  - start of using TOF in particle identification from $p_T = 0.7$ GeV/c,
  - $n_{\sigma_{TPC}} < 3$ for $p_T < 0.7$ GeV/c and $\sqrt{n^2_{\sigma_{TPC}} + n^2_{\sigma_{TOF}}} < 3$ otherwise,

- global tracks filter (called requireGlobalTrackInFilter()) – another build-in filter offering basic track cuts presented in table 3.1.

Table 3.1: Values for cuts in global track filter according to O^2 documentation [24].

Cuts	**Value in global tracks filter**
Minimum number of crossed rows in TPC	70
Minimum ratio of crossed rows over findable clusters in TPC	0.8
Maximum χ^2 of the vertex fit per TPC cluster	4
Maximum χ^2 per ITS cluster	36
Require TPC refit	true
Require ITS refit	true
Maximum distance of closest approach (DCA) to z coordinate of the vertex	2 cm
Maximum DCA to xy coordinates of the vertex	0.0105· 0.035 $/p_T^{11}$ cm
Cluster requirements for ITS	at least one hit in SPD for Run 2 data and at least one hit in 3 innermost ITS layers for Run 3 data
p_T range	$(0.1, 10^{10})$ GeV/c
η range	$(-0.8, 0.8)$

(Source: https://aliceo2group.github.io/analysis-framework/docs/basics-usage/HelperTasks.html#track-selection, O^2 documentation. Last accessed: 16.01.2024.)

- Rejection of a close pion pair if $\left((\Delta\phi^*_{av})^2/0.01^2 + \Delta\eta^2/(0.01\ (\text{cm}))^2\right) < 1$, where $(\Delta\phi^*_{av})^2$ is a value describing average angular difference between two tracks and $\Delta\eta$ is a difference of pseudorapidity.

Values of n_σ, used for particle identification, are given by the difference of the observed signal from a given detector from the expectations for a given particle (divided by the detector resolution) [21]. TOF measures time of flight of a particle and TPC measures energy loss dE/dx given theoretically by Bethe-Bloch curves. The choice of n_σ cuts comes from purity and efficiency analysis presented in the next section.

The chosen multiplicity and k_T ranges were inspired by the ALICE pion femtoscopy in p–p collisions paper from Run 1 [27]. Multiplicities ranges were: 1–11, 12–16, 17–22, 23–28, 29–34, 35–41, 42–51, 52–152, and k_T ranges were: 0.13–0.2 GeV/c, 0.2–0.3 GeV/c, 0.3–0.4 GeV/c, 0.4–0.5 GeV/c, 0.5–0.6 GeV/c, 0.6–0.7 GeV/c.

3.4. Purity and efficiency

Calculations of purity and efficiency using Monte Carlo datasets (simulations) anchored to analysed datasets can provide important guidance regarding particle identification (further also called PID).

Purity is the percentage of correctly identified particles. To calculate it I created histograms of PDG code of selected particles vs. their p_T. Then I divided number of particles of a given code – for pions 211 for π^+ and -211 for π^- [2] – by a total number of entries in a given p_T bin. PDG code is used in simulations and is unique to each particle. Example of such histograms for positive pions is shown in figure 3.1. It is noticeable that π^+ (PDG code 211) are most often confused with antimuons with PDG -13 accounting for 85.86% of misidentified particles, positrons with PDG -11 (9.76%), kaons with PDG 321 (4.26%), as well as sometimes with negative pions (PDG -211), protons (PDG 2212), muons (PDG 13) and positrons (PDG -11) all constituting less than 0.1% of wrongly identified particles.

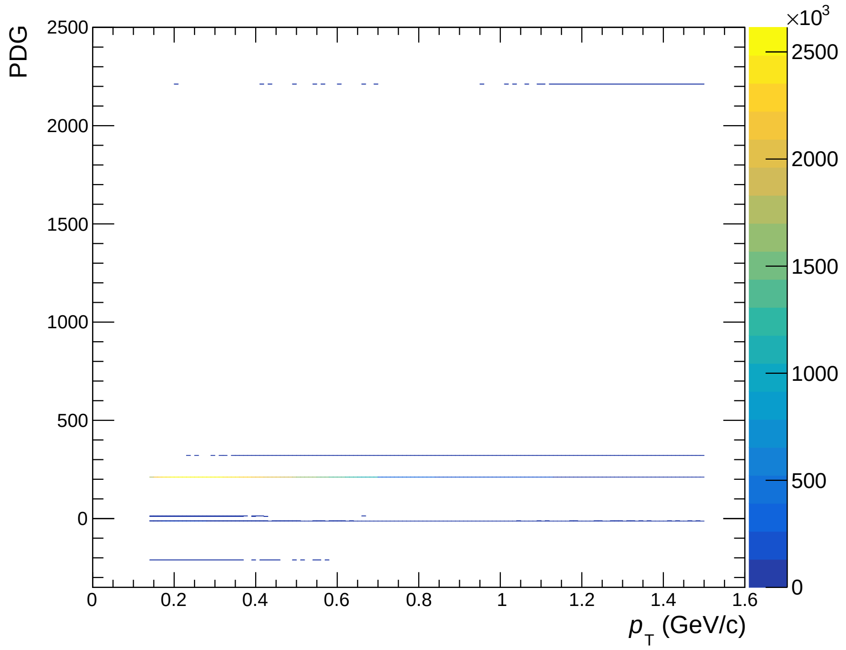

Figure 3.1: $PDG(p_T)$ histogram for positive pions for PYTHIA 8 p–p collisions at $\sqrt{s}$ = 13.6 TeV simulation anchored to Run 3.

If only TPC is used for PID purity drops drastically as shown for pions in figure 3.2 on the left. Figure 3.3 shows purity calculated with PID including TOF after p_T = 0.7 GeV/c. In this case purity for pions is above 95% (95.77% for π^+ and 95.75% for π^-).

Efficiency in high energy physics is understood is as the ratio of the number of particles detected and accepted by set selection to the actual number of particles of a given species created in a collision. When using only TPC for PID, efficiency takes value of around 70% as shown in figure 3.2 on the right. Including TOF in PID causes efficiency to decrease significantly, from aroud 70% to around 30% as visible on the right in figure 3.3. This is mainly due to low TOF matching efficiency (fraction of tracks with information from TOF). Other factors that have influence on efficiency are tracking efficiency defined as percentenge of particles registered by the detectors and PID efficiency, which tells about the amount of particles our PID selection rejects. Different efficiencies are shown in figure 3.4. TOF matching efficiency is only about 50%, causing full efficiency to drop. PID and tracking efficiency stay around 70%. Total efficiency takes values of 59.95% for π^+ and 59.83% for π^-.

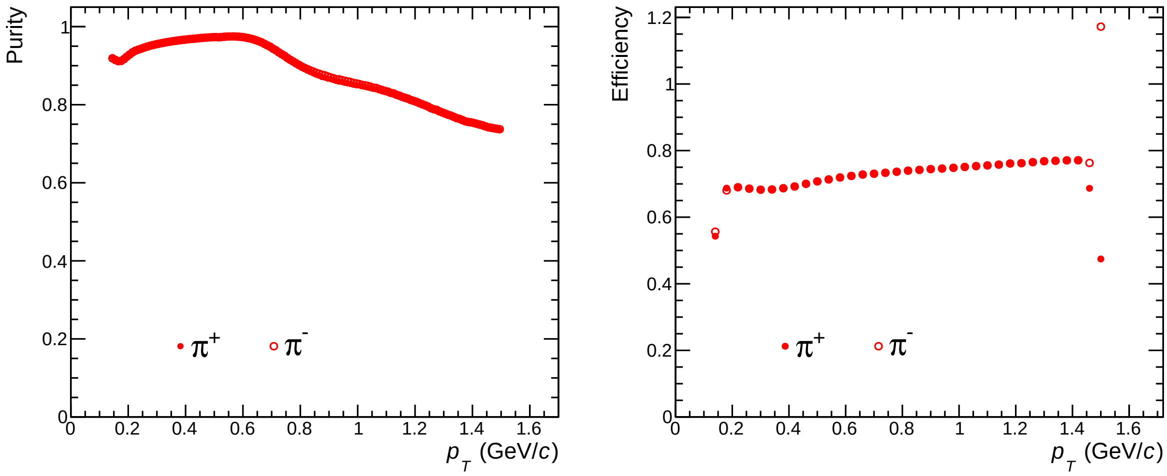

Figure 3.2: Purity and efficiency for pions for PYTHIA 8 p–p collisions at $\sqrt{s}$ = 13.6 TeV simulation anchored to Run 3 using only TPC for PID.

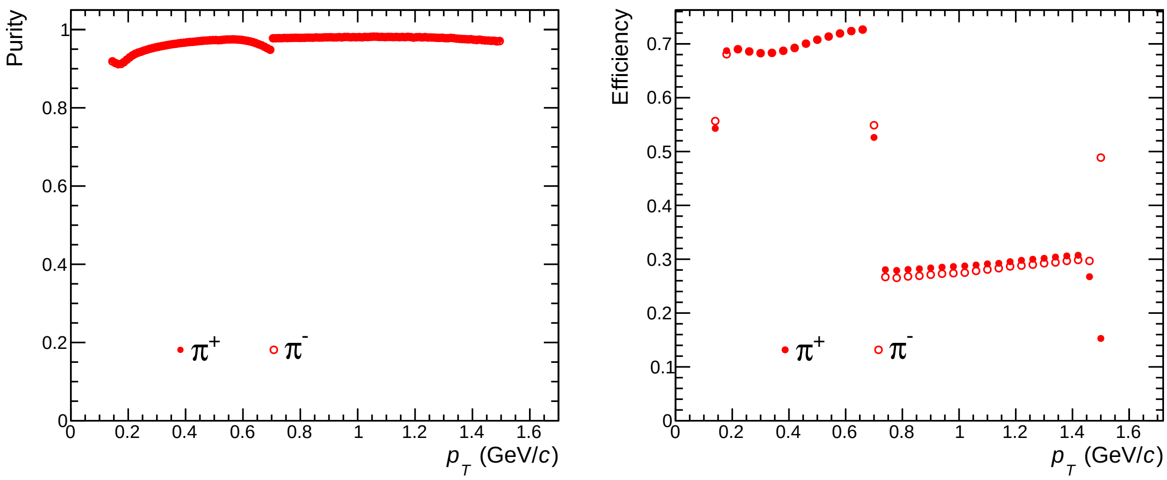

Figure 3.3: Purity and efficiency for pions for PYTHIA 8 p–p collisions at $\sqrt{s}$ = 13.6 TeV simulation anchored to Run 3.

It is important to choose a proper p_T threshold for including TOF in PID to balance good purity and efficiency and have good statistics. Based on presented purity and efficiency results I decided to choose p_T = 0.7 GeV/c.

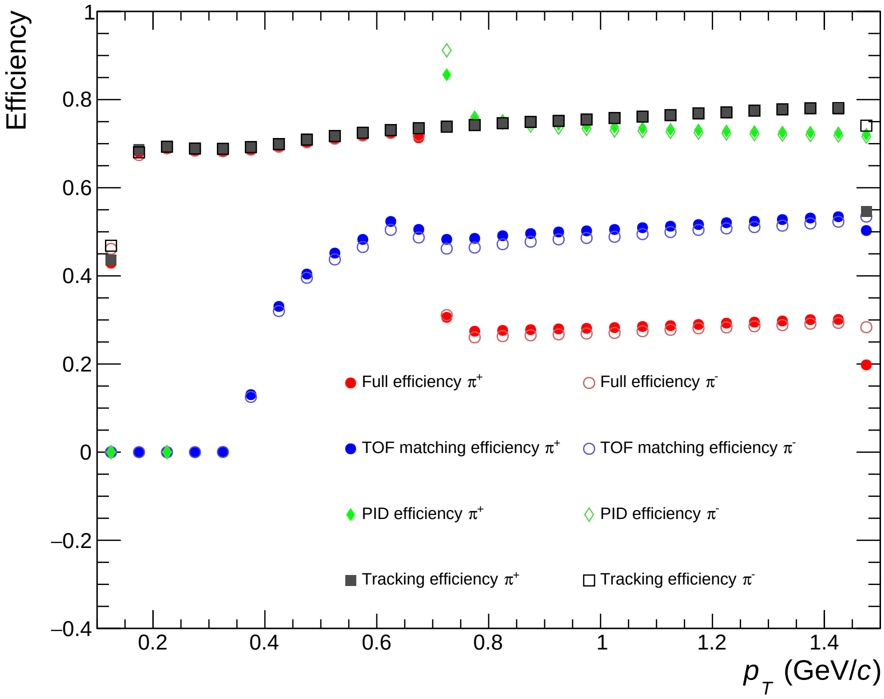

Figure 3.4: Efficiencies for pions for PYTHIA 8 p–p collisions at $\sqrt{s}$ = 13.6 TeV simulation anchored to Run 3.

3.5. Particle identification

Detectors that are mainly used for particle identification are TPC and TOF. n_σ histograms can show the quality of selection and suggest the appropriate choice of selection alongside purity and efficiency analysis.

Figures 3.5–3.10 show n_σ histograms for selected pions: 3.5 and 3.6 for Run 2 data, 3.7 and 3.9 for Run 3, 3.8 and 3.10 for MC simulations. There is no visible contamination from other particles. For n_σ^{TOF} histogram a moment where n_σ^{TOF} is started to be used for PID (p_T = 0.7 GeV/c, that gives larger value of momentum p) is visible. Due to a known problem in the O^2 software, n_σ histograms for TPC have incorrect binning and will be fixed in the future.

The dE/dx histograms for π^+ presented in figures 3.11 (for Run 2), 3.12 (for Run 3) and 3.13 (for MC) look as expected, there is only one Bethe-Bloch curve associated with pions.

In comparison with the data the n_σ distribution for MC is slightly shifted, although it should be almost the same for the anchored dataset. This might indicate that the quality of the MC datasets was not the best at the time the analysis was performed.

3.6. Quality assurance

In this section I present some other distributions for selected pions, which give valuable insight into the quality of data and selection. Applied cuts can be visible in p_T histograms shown in figures

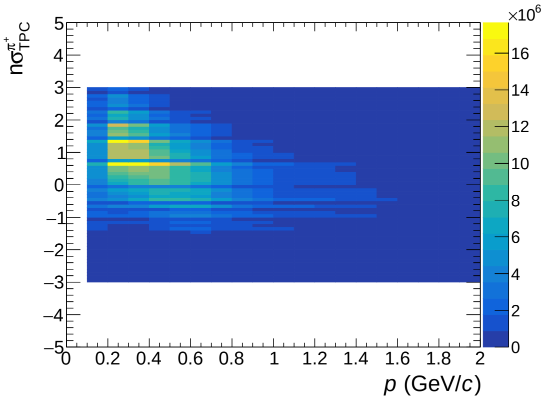

Figure 3.5: n_σ^{TPC} for positive pions for p–p collisions at $\sqrt{s}$ = 13 TeV data from Run 2.

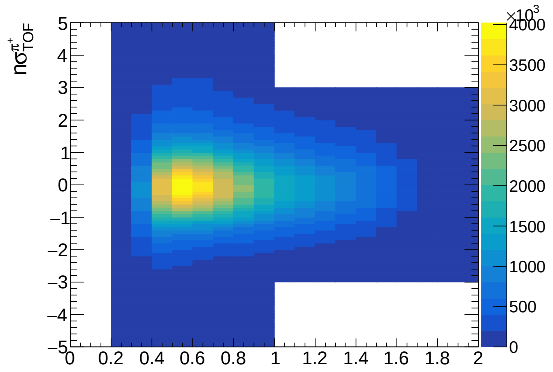

Figure 3.6: n_σ^{TOF} for positive pions for p–p collisions at $\sqrt{s}$ = 13 TeV data from Run 2.

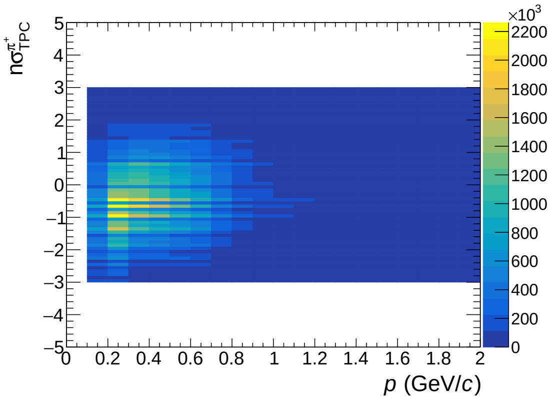

Figure 3.7: n_σ^{TPC} for positive pions for p–p collisions at $\sqrt{s}$ = 13.6 TeV data from Run 3.

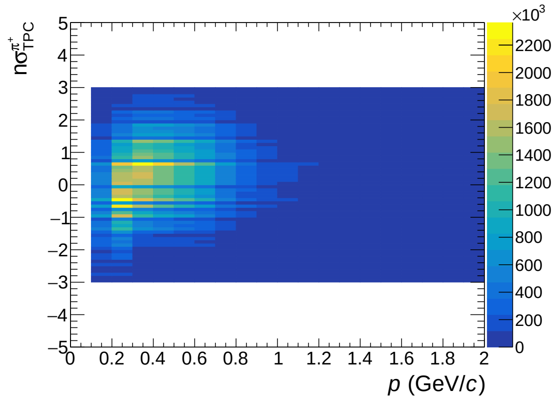

Figure 3.8: n_σ^{TPC} for positive pions for PYTHIA 8 p–p collisions at $\sqrt{s}$ = 13.6 TeV simulation anchored to Run 3.

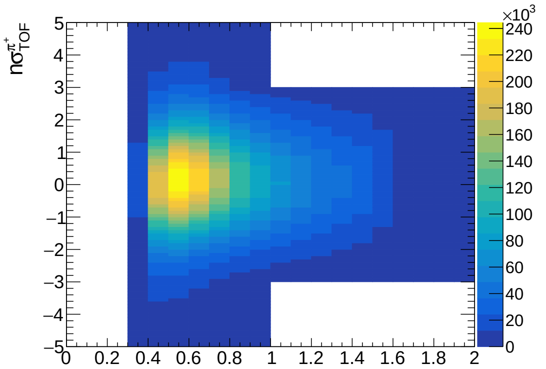

Figure 3.9: n_σ^{TOF} for positive pions for p–p collisions at $\sqrt{s}$ = 13.6 TeV data from Run 3.

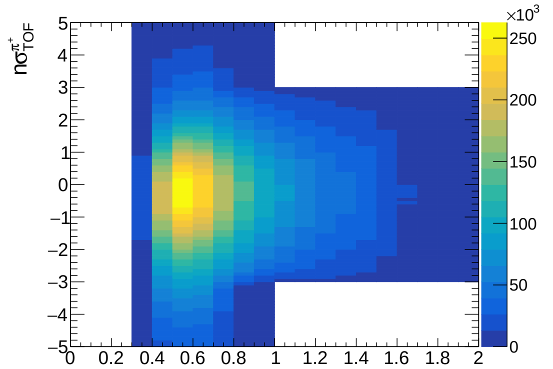

Figure 3.10: n_σ^{TOF} for positive pions for PYTHIA 8 p–p collisions at $\sqrt{s}$ = 13.6 TeV simulation anchored to Run 3.

3.15, 3.17 and 3.19 as well as η histograms shown in figures 3.14, 3.16 and 3.18 (distributions are shown for Run 2, Run 3 and MC simulations).

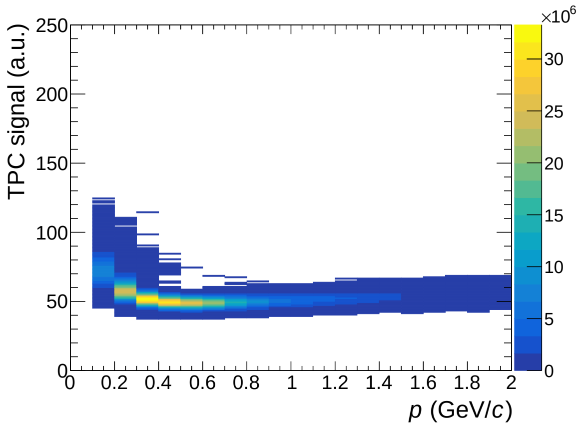

Figure 3.11: dE/dx from TPC for positive pions for p–p collisions at $\sqrt{s}$ = 13 TeV data from Run 2.

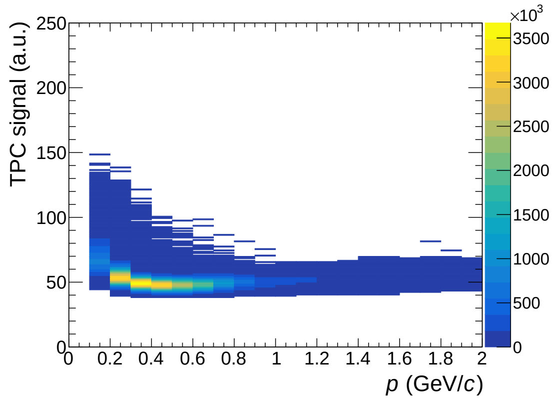

Figure 3.12: dE/dx from TPC for positive pions for p–p collisions at $\sqrt{s}$ = 13.6 TeV data from Run 3.

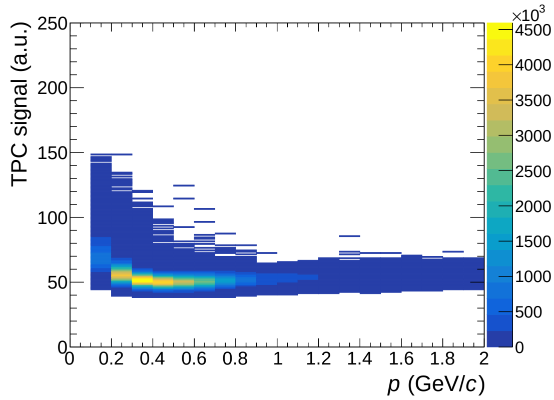

Figure 3.13: dE/dx from TPC for positive pions for PYTHIA 8 p–p collisions at $\sqrt{s}$ = 13.6 TeV simulation anchored to Run 3.

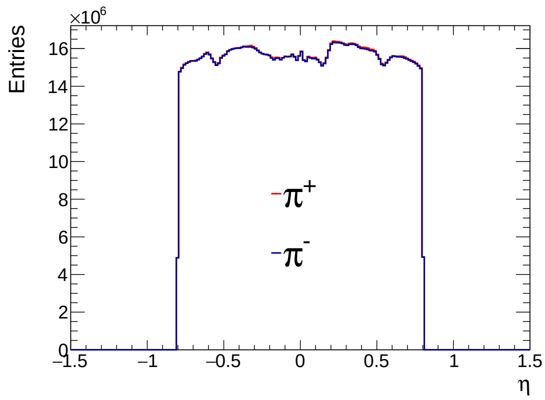

Figure 3.14: η for pions for p–p collisions at $\sqrt{s}$ = 13 TeV data from Run 2.

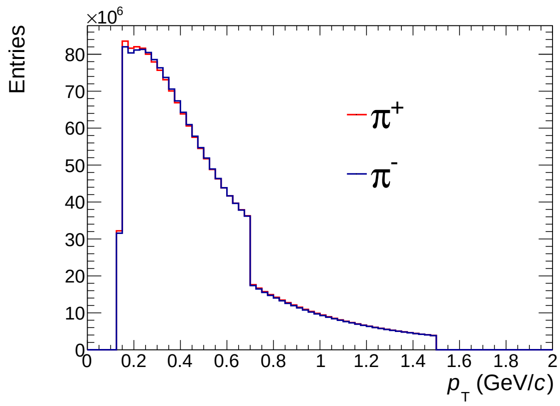

Figure 3.15: p_T for pions for p–p collisions at $\sqrt{s}$ = 13 TeV data from Run 2.

Multiplicity histograms are shown in figures 3.20 for Run 2, 3.21 for Run 3 and 3.22 for MC. There are mostly collisions with small multiplicity, but for Run 2 there is additional peak visible. This may be due to the use of a trigger that selects events with higher multiplicity for this dataset.

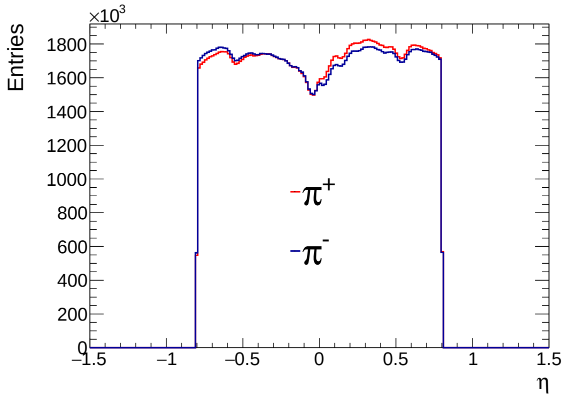

Figure 3.16: η for pions for p–p collisions at $\sqrt{s}$ = 13.6 TeV data from Run 3.

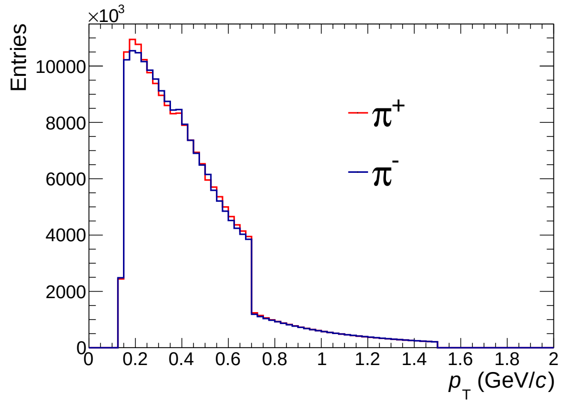

Figure 3.17: p_T for pions for p–p collisions at $\sqrt{s}$ = 13.6 TeV data from Run 3.

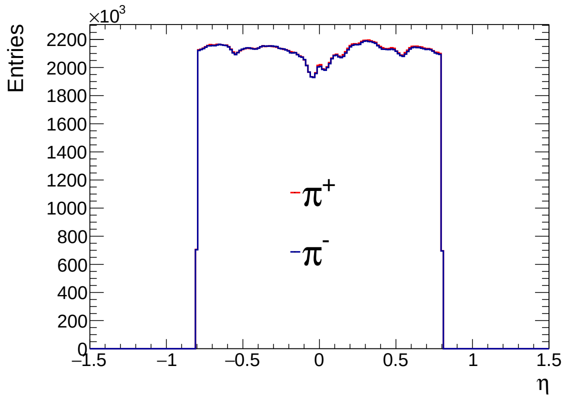

Figure 3.18: η for pions for PYTHIA 8 p–p collisions at $\sqrt{s}$ = 13.6 TeV simulation anchored to Run 3.

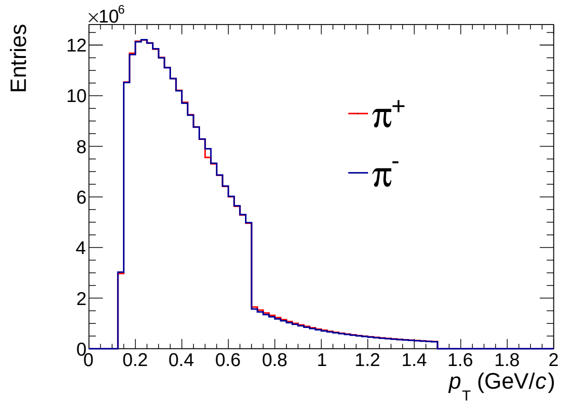

Figure 3.19: p_T for pions for PYTHIA 8 p–p collisions at $\sqrt{s}$ = 13.6 TeV simulation anchored to Run 3.

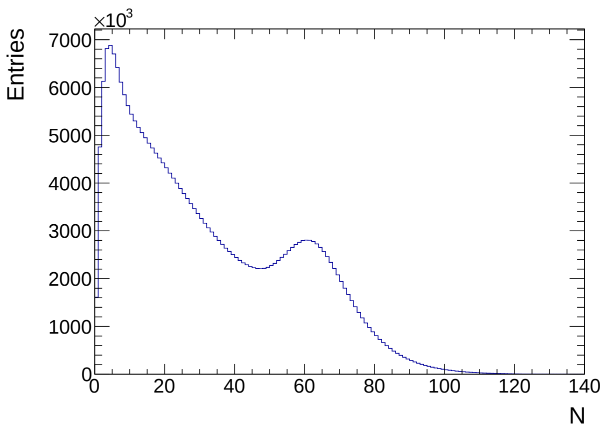

Figure 3.20: Multiplicity of events for p–p collisions at $\sqrt{s}$ = 13 TeV data from Run 2.

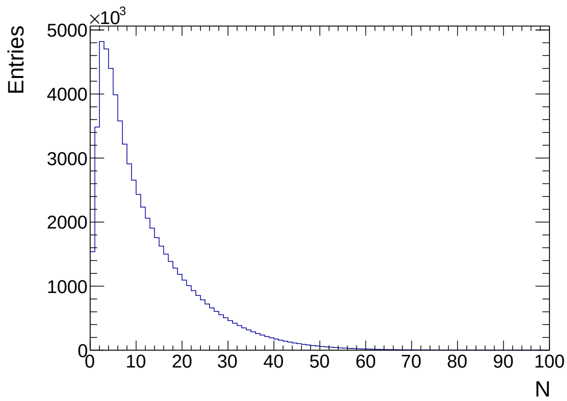

Figure 3.21: Multiplicity of events for p–p collisions at $\sqrt{s}$ = 13.6 TeV data from Run 3.

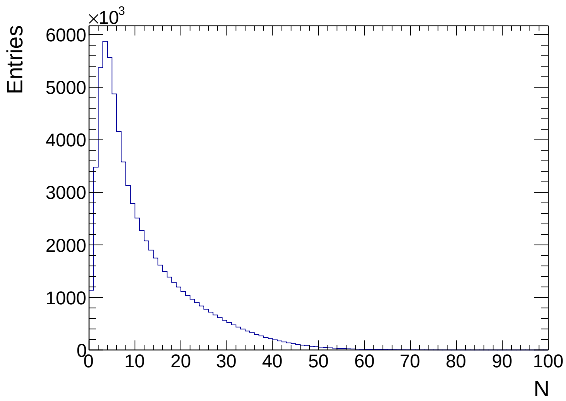

Figure 3.22: Multiplicity of events for PYTHIA 8 p–p collisions at $\sqrt{s}$ = 13.6 TeV simulation anchored to Run 3.

Chapter 4

Results

4.1. k^* histograms

Numerators and denominators of the pion–pion correlation functions for $\pi^+\pi^+$, $\pi^-\pi^-$ and $\pi^+\pi^-$ are shown in figures 4.1–4.6: 4.1 and 4.2 for Run 2, 4.3 and 4.4 for Run 3, 4.5 and 4.6 for MC. They can be looked at to check if they have correct shape and number of entries. Histograms of k^* for pions from mixed events have more entries than those for pions from the same event as events are being mixed with five others, as explained in section 3.1. For $\pi^+\pi^-$ resonance peak can be seen at around p_T = 0.2 GeV/c.

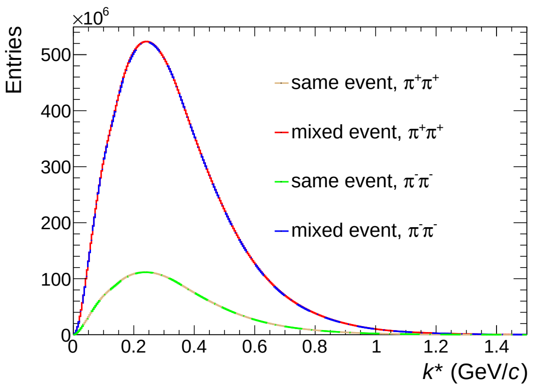

Figure 4.1: k^* histogram for $\pi^+\pi^+$ and $\pi^-\pi^-$ for p-p collisions at $\sqrt{s}$ = 13 TeV data from Run 2.

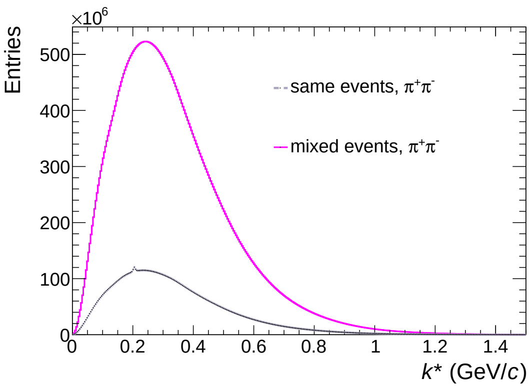

Figure 4.2: k^* histogram for $\pi^+\pi^-$ pions for p-p collisions at $\sqrt{s}$ = 13 TeV data from Run 2.

4.2. Correlation functions

Correlation functions calculated as explained in section 1.2 are shown in figure 4.7 for Run 2 is shown in figure 4.8 for Run 3.

Comparison between Run 3 datasets LHC22f_pass4 and LHC22o_pass4_minBias_small dataset is shown in figure 4.9. Similar results are expected as both of them contain data from p–p collisions at $\sqrt{s}$ = 13.6 TeV. Difference in interaction rate that is much smaller for LHC22f_pass4 should not cause many deviations. Correlation function for those datasets are almost the same with slight differences in the peak height and larger k^* range for which the function rises much more

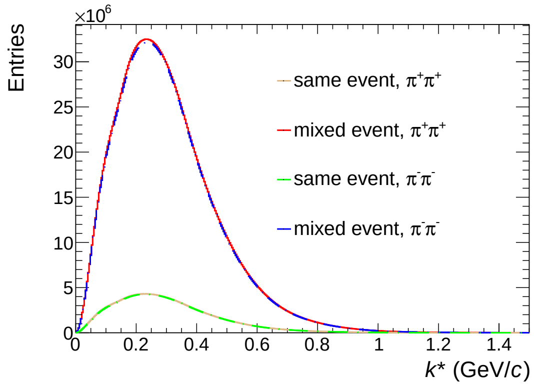

Figure 4.3: k^* histogram for $\pi^+\pi^+$ and $\pi^-\pi^-$ for p–p collisions at $\sqrt{s}$ = 13.6 TeV data from Run 3.

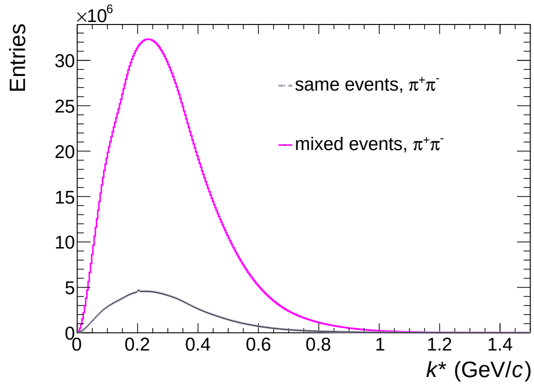

Figure 4.4: k^* histogram for $\pi^+\pi^-$ pions for p–p collisions at $\sqrt{s}$ = 13.6 TeV data from Run 3.

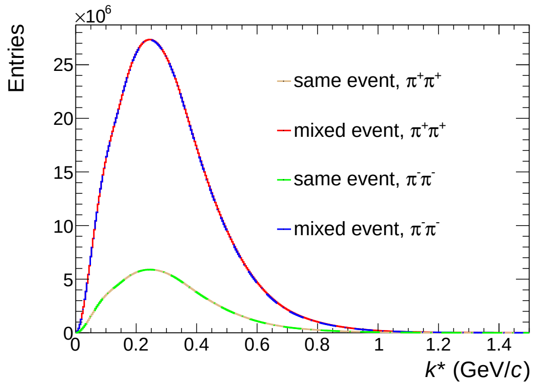

Figure 4.5: k^* histogram for $\pi^+\pi^+$ and $\pi^-\pi^-$ pions for PYTHIA 8 p–p collisions at $\sqrt{s}$ = 13.6 TeV simulation anchored to Run 3.

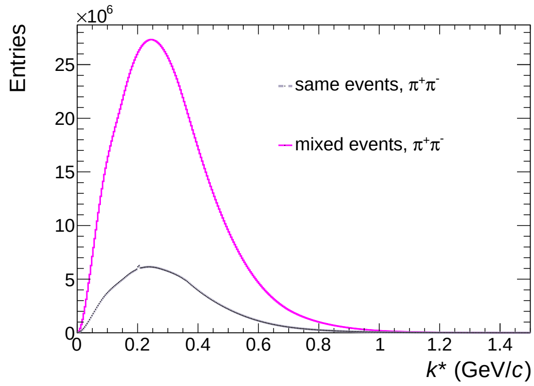

Figure 4.6: k^* histogram for $\pi^+\pi^-$ pions for PYTHIA 8 p–p collisions at $\sqrt{s}$ = 13.6 TeV simulation anchored to Run 3.

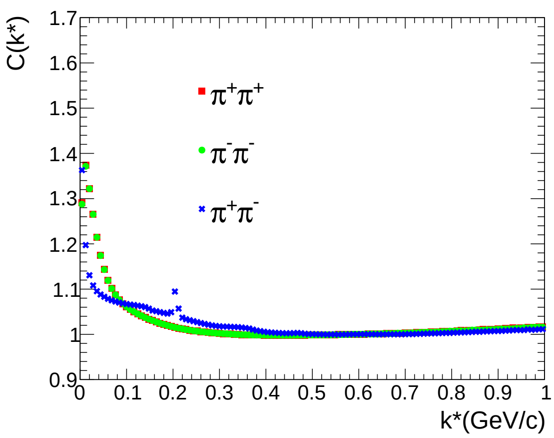

Figure 4.7: Correlation functions for p–p collisions at $\sqrt{s}$ = 13 TeV data from Run 2.

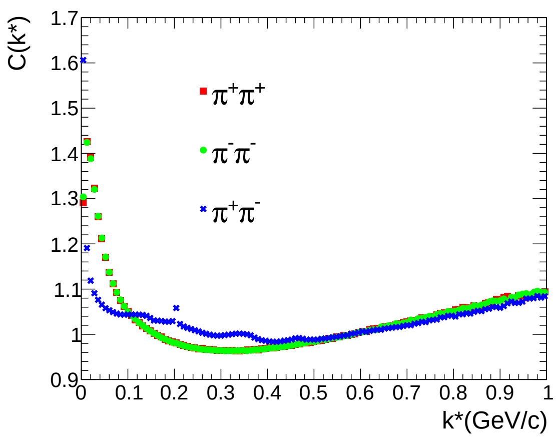

Figure 4.8: Correlation functions for p–p collisions at $\sqrt{s}$ = 13.6 TeV data from Run 3.

for LHC22o_pass4_minBias_small. For the clarity of this thesis most of the rest of the results are presented for LHC22f_pass4 dataset (as already mentioned in section 2.4) and for positive pions, as they do not differ significantly from negative pions. The results for LHC22o_pass4_minBias_small are presented in the appendix A.

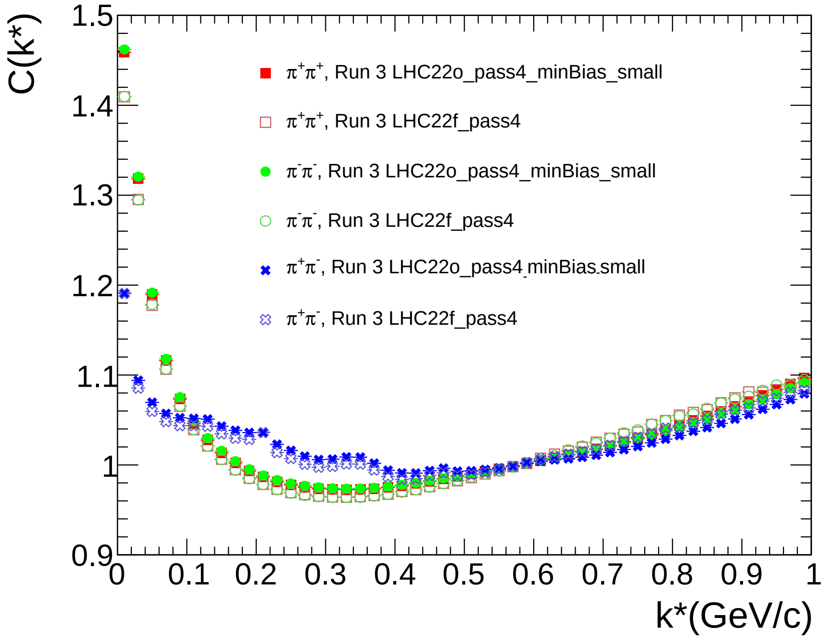

Figure 4.9: Comparison of correlation functions for $\pi^+\pi^+$ for LHC22f_pass4 and LHC22f_pass4_small datasets for p–p collisions at $\sqrt{s}$ = 13.6 from Run 3.

The shape of the obtained correlation functions matches theoretical expectations and shows the influence of various physical effects. For low values of k^* $\pi^+\pi^+$ and $\pi^-\pi^-$ function descends, while for $\pi^+\pi^-$ rises. This is the effect of the Coulomb interactions, which are negative for the same charged particles, and positive for those with opposite signs. The functions for $\pi^+\pi^+$ and $\pi^-\pi^-$ are almost identical, as expected, there should be no difference between them. The femtoscopic effects from Bose-Einstein correlations are very well visible for k^* smaller than 0.2 GeV/c. For the $\pi^+\pi^-$ function resonance peaks are observed with especially prominent peak at around $k^* = 0.2$ GeV/c.

The comparison of correlation functions for the Run 2 and Run 3 is shown in figure 4.10. They differ for same charged pions. For higher k^* function for p–p collisions at $\sqrt{s} = 13$ TeV data from Run 2 is above function for collisions at $\sqrt{s} = 13.6$ TeV data from Run 3, as opposed to k^* interval of around $0.1 - 0.5$ GeV/c for which it is below. This is to be expected as matters like detectors settings may be different for different data sets. Also used dataset from Run 2 contains more high multiplicity events what can have an impact on the results. However, the width of the correlation function is comparable. Results for $\pi^+\pi^-$ for both datasets match better for lower k^*, but there are similar differences for higher k^* as for $\pi^+\pi^+$ and $\pi^-\pi^-$.

I also calculated correlation functions for different multiplicity ranges and the results are shown in figure 4.11. The most important thing to note is that the width of the correlation function decreases with the multiplicity. This corresponds to the increasing size of the source, as it is inversely proportional. This figure also shows much better than figure 4.8 that the correlation function rises for

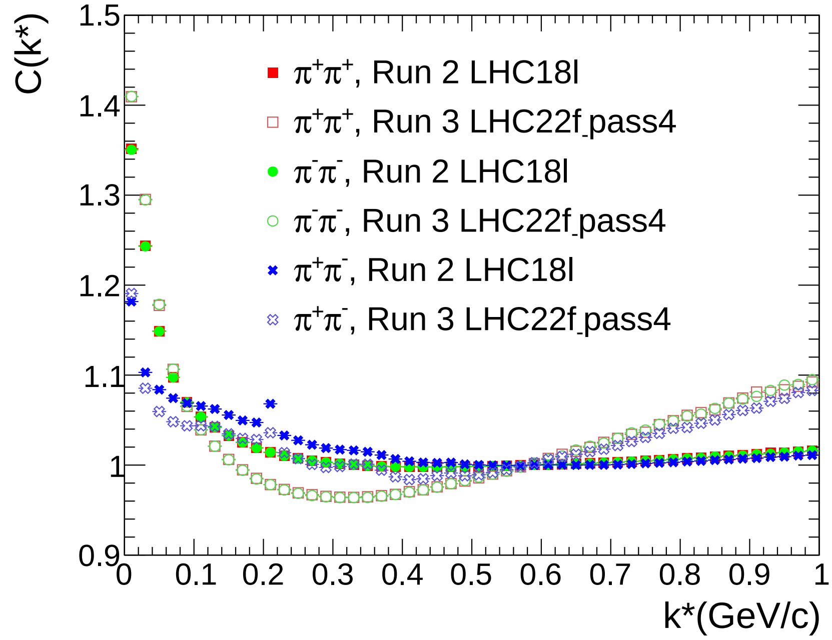

Figure 4.10: Comparison of correlation functions for $\pi^+\pi^+$ for p–p collisions at $\sqrt{s}$ = 13.6 TeV data from Run 3 and p–p collisions at $\sqrt{s}$ = 13 TeV data from Run 2.

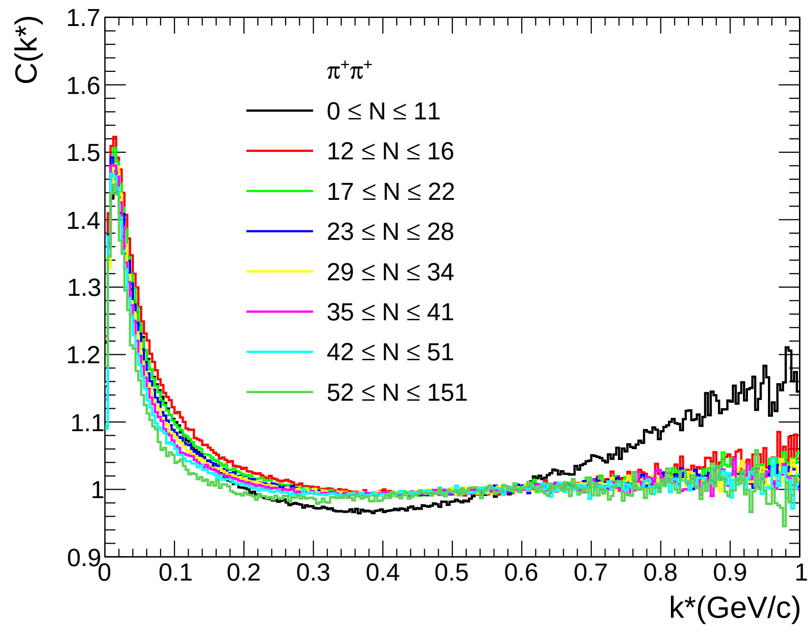

Figure 4.11: Correlation functions for $\pi^+\pi^+$ for p–p collisions at $\sqrt{s}$ = 13.6 TeV data from Run 3 for different multiplicities ranges.

higher k^*, especially for low multiplicity $0 \leqslant N \leqslant 11$, marked in black. It is expected behaviour caused by conservation laws that have bigger impact on the shape of the correlation function in lower multiplicity events [28].

For different multiplicities I calculated correlation functions for different k_T ranges. They are presented in figure 4.12.

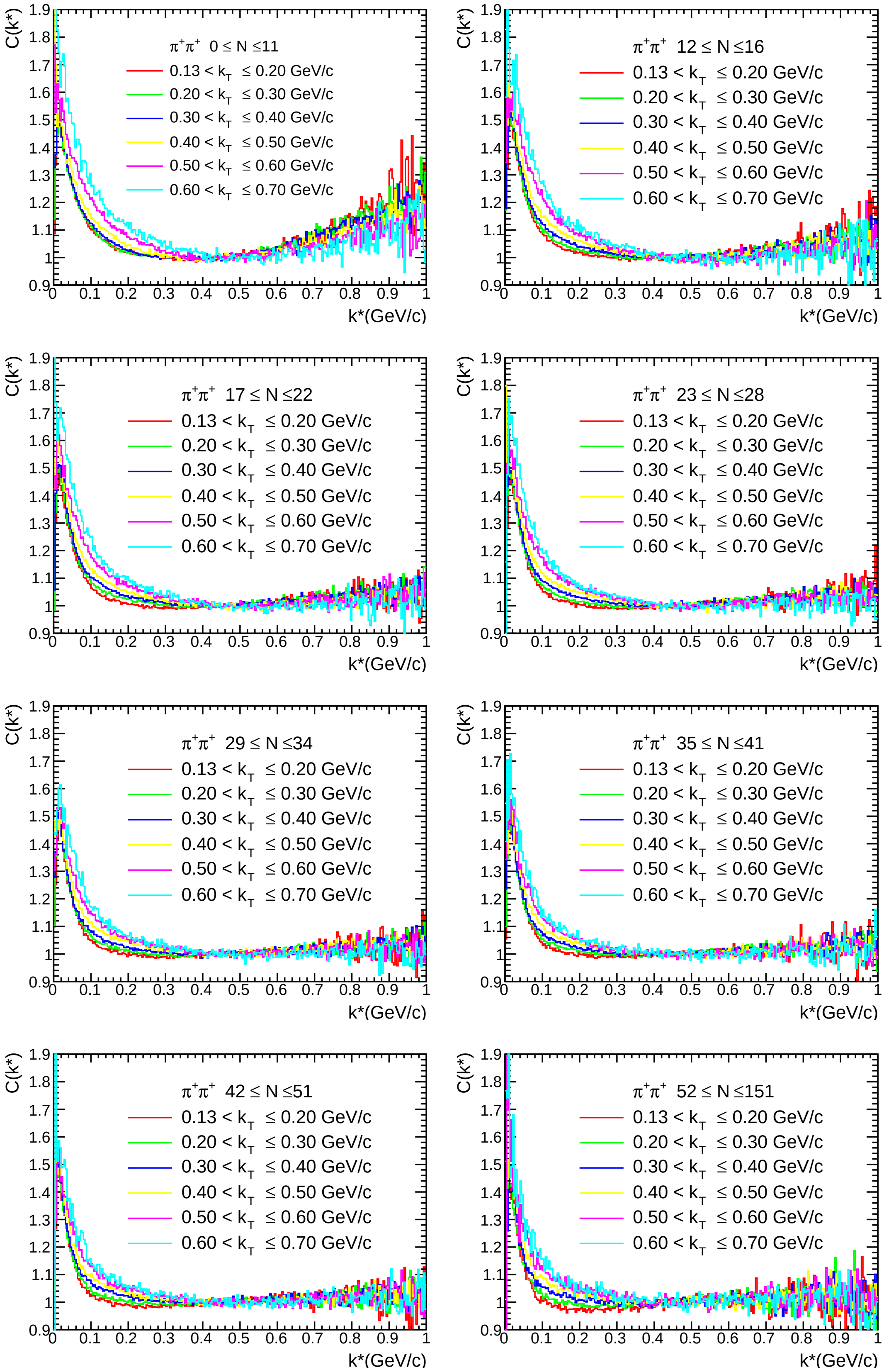

Figure 4.12: Correlation functions for p–p collisions at $\sqrt{s}$ = 13.6 TeV data from Run 3 for different multiplicities and k_T ranges.

In this case the larger k_T range, the wider the correlation function, which corresponds to decreasing source size.

Results presented in figures 4.7-4.12 include the background. As mentioned earlier in section 1.2 there are two options of background removal – using Monte Carlo simulation or applying sphericity cut. In this thesis I used the first method. The process is presented in section 4.2.1.

4.2.1. Background

PYTHIA 8 simulations that I used do not include effects of Bose-Einstein correlations, but they reproduce other effects well, which allows their use in background removal. The comparison between the $\pi^+\pi^+$ results of the same analysis for MC and for real data datasets is shown in figures 4.13. As expected, due to the lack of femtoscopic effects in the simulations, the MC results are much flatter for smaller k^*. For higher k^*, especially for smaller multiplicities data and MC functions do not match well.

Figure 4.14 shows results for PYTHIA 8 simulation anchored to Run 3 in different multiplicity and k_T ranges. It can be compared with figure 4.12 for data from Run 3.

In order to properly estimate the background without propagating the statistical fluctuations in MC results I fitted them with a fifth degree polynomial (I fitted them in range $k^* \in [0.01; 0.5]$). I then divided the correlation function by this polynomial, resulting in correlation functions that should only include the effects we intend to study, without the influence of conservation laws etc. These are presented in the next section.

4.2.2. Fitting

After removing the background I fitted the correlation functions with both exponential (equation 1.7) and Gaussian (equation 1.6) functions to obtain the information about the source size R and the correlation strength λ. I used the calculated Coulumb function $K(k^*)$ from the macro previously developed in the ALICE WUT group by prof. Adam Kisiel [29]. Since the small $K(k^*)$ does not change significantly for small changes in R I used it for $R = 1.2$ fm. It is shown in figure 4.15.

To get the best results I fitted functions for k^* from 0 to 0.2 GeV/c. It is important to note that for higher multiplicities, as well as for higher k_T, the statistics are smaller, resulting in a worse fit and less accurate R calculations. The exemplary fit results are shown in figure 4.16.

The exponential fit reflects the correlation functions noticably better than the Gaussian fit, which provides information about the shape of the source.

4.3. Source size

Figure 4.19 and figure 4.18 show the obtained source sizes R respectively for the exponential and Gaussian fit. The uncertainties given represent only the fit uncertainties. The largest multiplicity

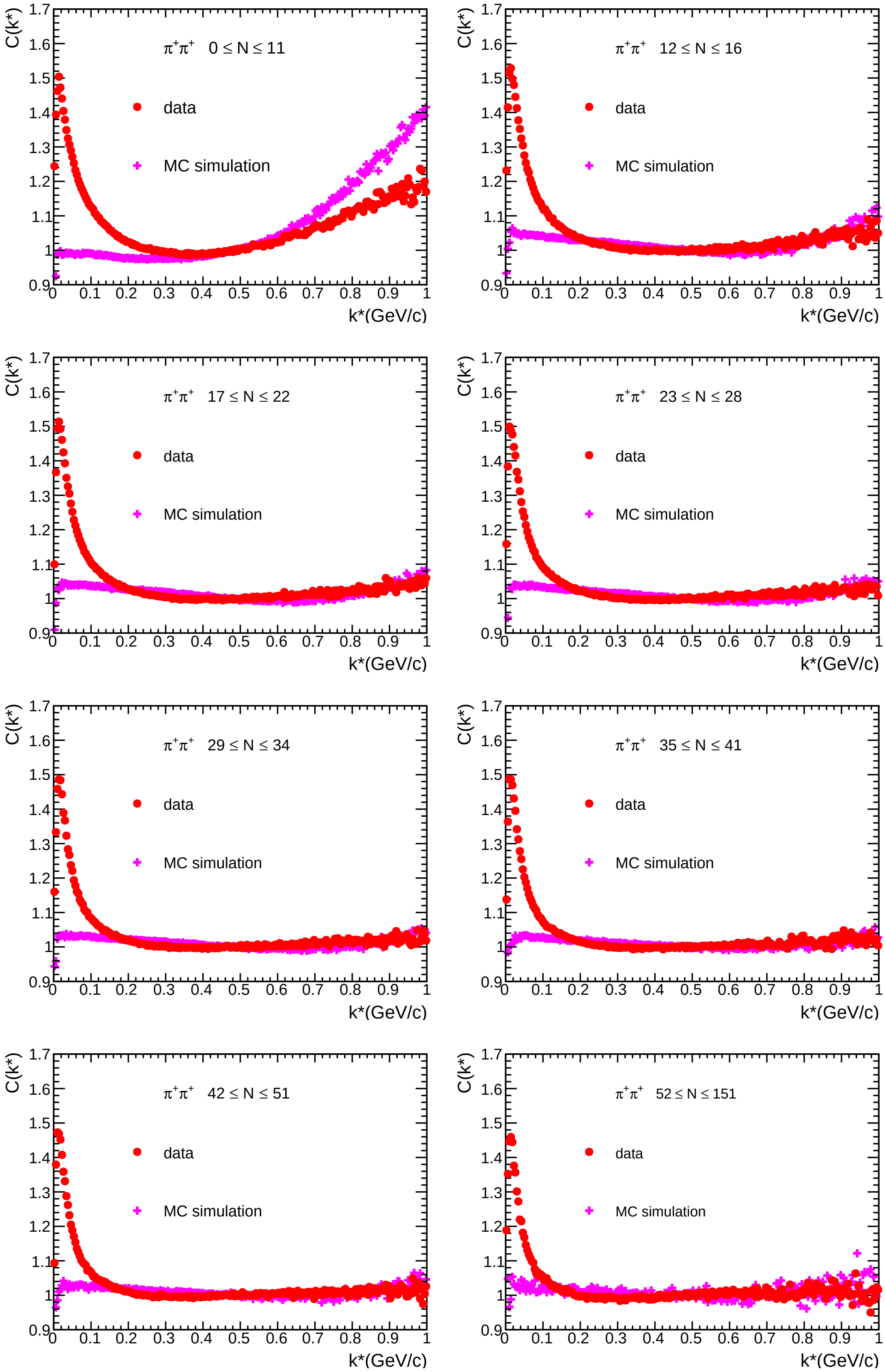

Figure 4.13: Correlation functions comparison for p–p collisions at $\sqrt{s}$ = 13.6 TeV data from Run 3 and PYTHIA 8 p–p collisions at $\sqrt{s}$ = 13.6 TeV simulation anchored to Run 3 for positive pions.

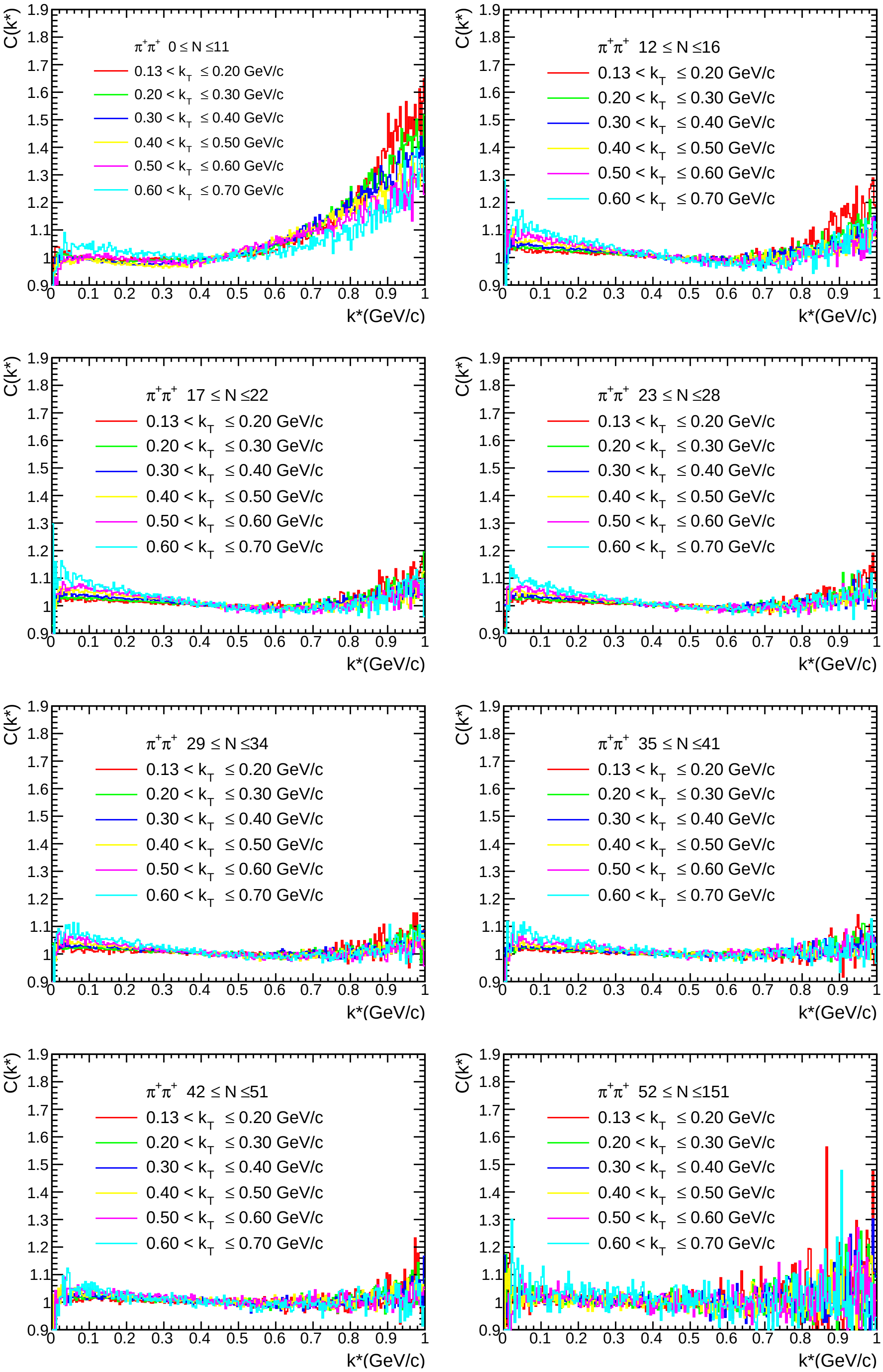

Figure 4.14: Correlation functions for PYTHIA 8 simulation anchored to Run 3 for positive pions for different multipliciy and k_T ranges.

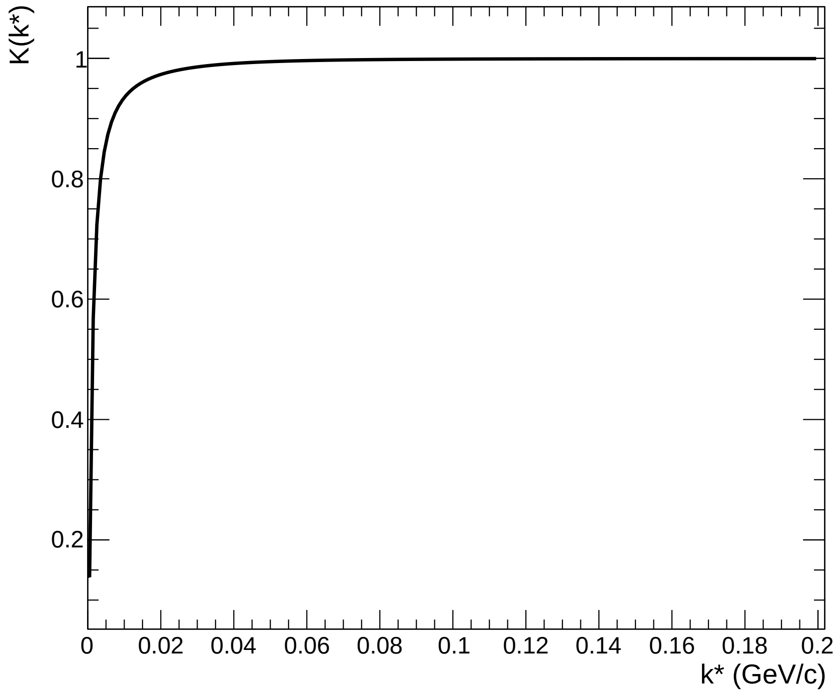

Figure 4.15: Coulumb function $K(k^*)$ for $R = 1.2$ fm.

range $51 \leqslant N \leqslant 151$ has smaller statistics resulting in poorer fit quality what can cause the R values in this N interval to stand out the most from the general trend.

In order to compare results of Gaussian and exponential, fit parameters obtained for the latter have to be divided by $\sqrt{\pi}$ [5]. The figure 4.19 shows source sizes R for the exponential fit after scaling. In this section and in table 4.1 scaled values are presented.

For exponential fit R takes values in the range of 0.6459 ± 0.0090 fm to 2.466 ± 0.068 fm. For Gaussian fit R takes values from 0.7221 ± 0.0064 fm to 2.25 ± 0.053 fm. As previously predicted from the correlation functions, R becomes smaller with increasing k_T and larger with increasing multiplicity N although there are few exceptions for $k_T > 0.5$ GeV/c. Also, for $k_T > 0.6$ GeV/c R is larger than for the previous k_T intervals. These observations may be partially due to lower statistics in these larger ranges affecting the quality of the fit.

For the exponential fit the λ parameter takes values in the range 0.282 ± 0.015 to 0.589 ± 0.041. For Gaussian fit λ takes values from 0.218 ± 0.013 to 0.469 ± 0.028. Full results of R and λ are presented in table 4.1.

Table 4.1: Results of exponential (scaled by $\sqrt{\pi}$) and Gaussian fit of the correlation function.

1 k_T	2 R_{exp} fm	3 λ_{exp}	4 R_{gaus} fm	5 λ_{gaus}
$0 \leqslant N \leqslant 11$				
$0.13 < k_T \leqslant 0.20$	0.8962 ± 0.0093	0.3242 ± 0.0042	0.9438 ± 0.0073	0.3227 ± 0.0035
$0.20 < k_T \leqslant 0.30$	0.8448 ± 0.0062	0.3155 ± 0.0028	0.8937 ± 0.0047	0.3094 ± 0.0021

1	2	3	4	5
$0.30 < k_T \leqslant 0.40$	0.7393 ± 0.0066	0.3001 ± 0.0033	0.7762 ± 0.0047	0.2865 ± 0.0023
$0.40 < k_T \leqslant 0.50$	0.6442 ± 0.0071	0.3167 ± 0.0040	0.7098 ± 0.0050	0.3195 ± 0.0029
$0.50 < k_T \leqslant 0.60$	0.6459 ± 0.0090	0.3923 ± 0.0063	0.7221 ± 0.0064	0.4061 ± 0.0048
$0.60 < k_T \leqslant 0.70$	0.675 ± 0.014	0.458 ± 0.012	0.7282 ± 0.0098	0.4522 ± 0.0088
$11 \leqslant N \leqslant 16$				
$0.13 < k_T \leqslant 0.20$	1.329 ± 0.015	0.3990 ± 0.0064	1.346 ± 0.013	0.3802 ± 0.0053
$0.20 < k_T \leqslant 0.30$	1.293 ± 0.011	0.3939 ± 0.0048	1.2814 ± 0.0086	0.3523 ± 0.0035
$0.30 < k_T \leqslant 0.40$	1.150 ± 0.012	0.3603 ± 0.0055	1.1182 ± 0.0090	0.3099 ± 0.0040
$0.40 < k_T \leqslant 0.50$	1.024 ± 0.013	0.3509 ± 0.0066	1.0021 ± 0.0099	0.3053 ± 0.0047
$0.50 < k_T \leqslant 0.60$	0.849 ± 0.014	0.3601 ± 0.0078	0.8835 ± 0.0099	0.3468 ± 0.0058
$0.60 < k_T \leqslant 0.70$	0.834 ± 0.020	0.396 ± 0.013	0.871 ± 0.014	0.384 ± 0.010
$17 \leqslant N \leqslant 22$				
$0.13 < k_T \leqslant 0.20$	1.529 ± 0.016	0.4325 ± 0.0064	1.516 ± 0.013	0.4021 ± 0.0051
$0.20 < k_T \leqslant 0.30$	1.372 ± 0.010	0.4022 ± 0.0045	1.3627 ± 0.0084	0.3589 ± 0.0034
$0.30 < k_T \leqslant 0.40$	1.247 ± 0.012	0.3670 ± 0.0053	1.1938 ± 0.0094	0.3065 ± 0.0039
$0.40 < k_T \leqslant 0.50$	1.140 ± 0.013	0.3655 ± 0.0065	1.0944 ± 0.0101	0.3082 ± 0.0046
$0.50 < k_T \leqslant 0.60$	0.941 ± 0.014	0.3639 ± 0.0075	0.9515 ± 0.0103	0.3359 ± 0.0056
$0.60 < k_T \leqslant 0.70$	0.880 ± 0.019	0.387 ± 0.012	0.894 ± 0.013	0.3614 ± 0.0087
$23 \leqslant N \leqslant 28$				
$0.13 < k_T \leqslant 0.20$	1.649 ± 0.018	0.4502 ± 0.0072	1.649 ± 0.015	0.4216 ± 0.0058
$0.20 < k_T \leqslant 0.30$	1.518 ± 0.012	0.4157 ± 0.0052	1.482 ± 0.010	0.3619 ± 0.0038
$0.30 < k_T \leqslant 0.40$	1.319 ± 0.013	0.3713 ± 0.0059	1.266 ± 0.011	0.3108 ± 0.0044
$0.40 < k_T \leqslant 0.50$	1.124 ± 0.014	0.3406 ± 0.0065	1.091 ± 0.011	0.2913 ± 0.0048
$0.50 < k_T \leqslant 0.60$	0.882 ± 0.015	0.3205 ± 0.0071	0.897 ± 0.011	0.2974 ± 0.0052
$0.60 < k_T \leqslant 0.70$	0.943 ± 0.021	0.389 ± 0.013	0.933 ± 0.015	0.3493 ± 0.0092
$29 \leqslant N \leqslant 34$				
$0.13 < k_T \leqslant 0.20$	1.699 ± 0.021	0.4484 ± 0.0081	1.683 ± 0.017	0.4145 ± 0.0065
$0.20 < k_T \leqslant 0.30$	1.628 ± 0.015	0.4379 ± 0.0063	1.578 ± 0.012	0.3762 ± 0.0046
$0.30 < k_T \leqslant 0.40$	1.436 ± 0.017	0.3813 ± 0.0073	1.351 ± 0.013	0.3093 ± 0.0052
$0.40 < k_T \leqslant 0.50$	1.078 ± 0.016	0.3078 ± 0.0068	1.042 ± 0.013	0.2613 ± 0.0049
$0.50 < k_T \leqslant 0.60$	0.983 ± 0.018	0.3334 ± 0.0087	0.976 ± 0.014	0.2992 ± 0.0063
$0.60 < k_T \leqslant 0.70$	0.964 ± 0.024	0.365 ± 0.013	0.968 ± 0.018	0.338 ± 0.010
$35 \leqslant N \leqslant 41$				
$0.13 < k_T \leqslant 0.20$	1.844 ± 0.025	0.490 ± 0.010	1.796 ± 0.020	0.4399 ± 0.0077
$0.20 < k_T \leqslant 0.30$	1.727 ± 0.018	0.4574 ± 0.0077	1.673 ± 0.014	0.3908 ± 0.0056
$0.30 < k_T \leqslant 0.40$	1.390 ± 0.018	0.3615 ± 0.0077	1.335 ± 0.015	0.3024 ± 0.0057

1	2	3	4	5
$0.40 < k_T \leqslant 0.50$	1.161 ± 0.019	0.3338 ± 0.0082	1.115 ± 0.015	0.2804 ± 0.0059
$0.50 < k_T \leqslant 0.60$	1.033 ± 0.021	0.3360 ± 0.0099	1.019 ± 0.016	0.2995 ± 0.0072
$0.60 < k_T \leqslant 0.70$	1.074 ± 0.031	0.386 ± 0.017	1.052 ± 0.025	0.341 ± 0.013
$42 \leqslant N \leqslant 51$				
$0.13 < k_T \leqslant 0.20$	2.074 ± 0.034	0.518 ± 0.013	1.988 ± 0.027	0.4567 ± 0.0099
$0.20 < k_T \leqslant 0.30$	1.886 ± 0.024	0.455 ± 0.010	1.774 ± 0.019	0.3736 ± 0.0068
$0.30 < k_T \leqslant 0.40$	1.471 ± 0.024	0.367 ± 0.010	1.382 ± 0.019	0.2955 ± 0.0071
$0.40 < k_T \leqslant 0.50$	1.278 ± 0.026	0.348 ± 0.011	1.228 ± 0.022	0.2890 ± 0.0086
$0.50 < k_T \leqslant 0.60$	1.077 ± 0.026	0.342 ± 0.012	1.053 ± 0.019	0.3009 ± 0.0087
$0.60 < k_T \leqslant 0.70$	0.965 ± 0.033	0.363 ± 0.018	0.928 ± 0.025	0.309 ± 0.013
$52 \leqslant N \leqslant 151$				
$0.13 < k_T \leqslant 0.20$	2.466 ± 0.068	0.506 ± 0.024	2.225 ± 0.052	0.417 ± 0.017
$0.20 < k_T \leqslant 0.30$	2.124 ± 0.048	0.451 ± 0.018	1.948 ± 0.037	0.355 ± 0.012
$0.30 < k_T \leqslant 0.40$	1.692 ± 0.047	0.393 ± 0.019	1.579 ± 0.038	0.312 ± 0.014
$0.40 < k_T \leqslant 0.50$	1.044 ± 0.037	0.282 ± 0.015	0.958 ± 0.029	0.218 ± 0.010
$0.50 < k_T \leqslant 0.60$	0.997 ± 0.037	0.350 ± 0.019	0.961 ± 0.028	0.297 ± 0.013
$0.60 < k_T \leqslant 0.70$	1.219 ± 0.050	0.589 ± 0.041	1.124 ± 0.038	0.469 ± 0.028

4.4. Comparison with published articles

Presented results can be compared with already published articles. I will refer to "Femtoscopic correlations of identical charged pions and kaons in pp collisions at $\sqrt{s} = 13$ TeV with event-shape selection" by ALICE Collaboration published in 2023 [5]. The results are not directly comparable, as parameters such as multiplicity and k_T intervals as well as the methods of background removal are different. The article uses a sphericity cut alongside use of MC (PYTHIA 8) data. However, the results can be compared qualitatively. The figure 4.20 shows exemplary correlation function for same charged pions obtained by the authors of this article with both femtoscopic and Gaussian fit. They are in a function of $q_{inv} = \sqrt{q^2 - q_0^2}$ where q is related to k^* by $q = 2 \cdot k^*$ [3] and q_0 is the difference of particles energies [5]. The shape of the correlation function matches results I previously presented. The function height is around 1.5 and the femtoscopic effect for presented multiplicity and k_T intervals is visible for $q_{inv} < 0.2$ GeV/c. Similarly to my fit results in figure 4.16, exponential fit is more suitable for these correlation function.

Figure 4.21 shows source size R_{inv} obtained by the authors of this article. It is presented in different ranges of m_T that scales to k_T by equation 1.4. Similar dependence is observed: R_{inv} increases with multiplicity and decreases with m_T (or k_T). R_{inv} takes values in the range of around 0.5-2.0 fm which mostly coincides with my calculations, with the exception of two largest multiplicities which is expected, as authors of articles used wide range of $N > 30$.

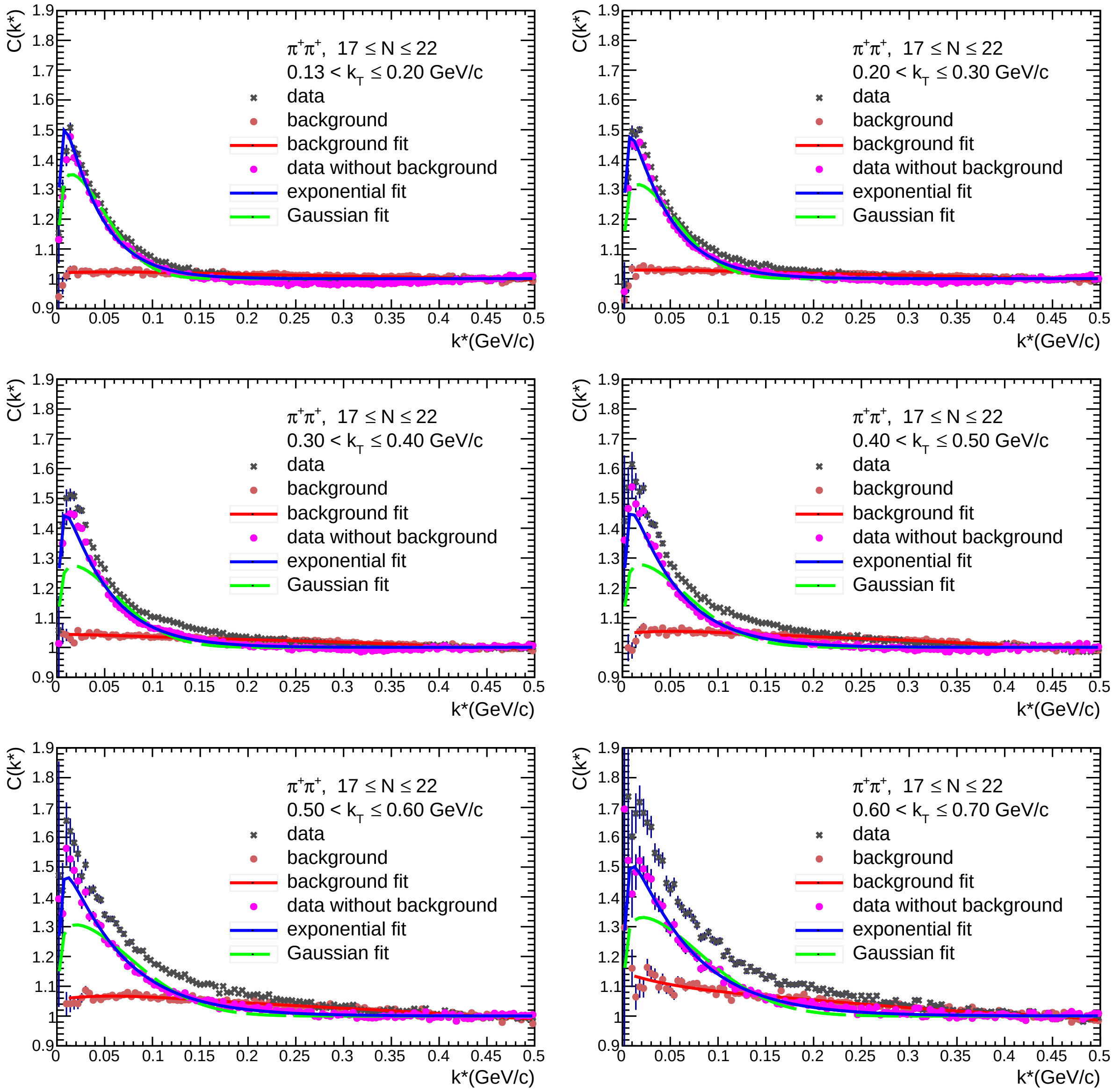

Figure 4.16: Fit results for positive pions for Run 3 data in multiplicity range $17 \leqslant N \leqslant 22$

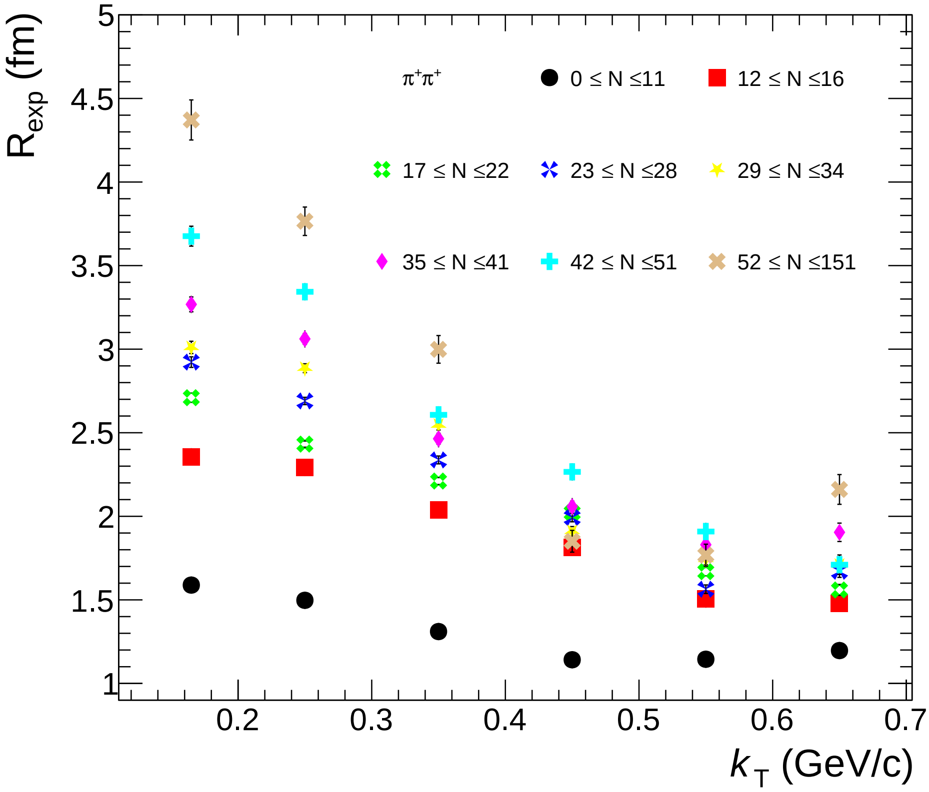

Figure 4.17: Source size *R* calculated for positive pions for Run 3 data from exponential fit.

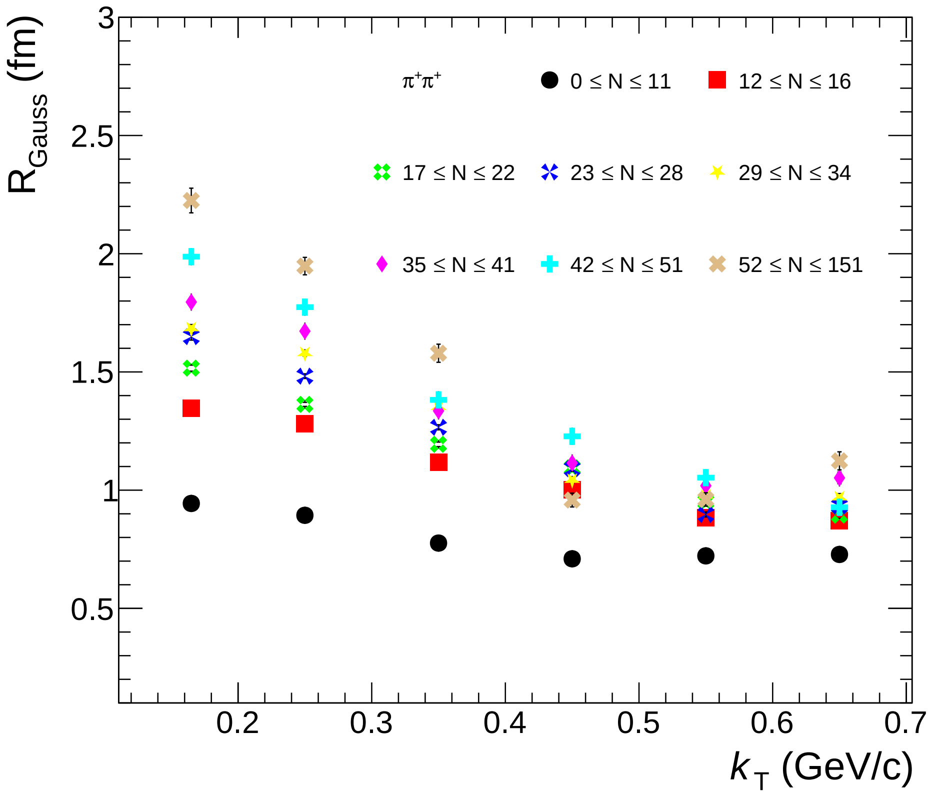

Figure 4.18: Source size *R* calculated for positive pions for Run 3 data from Gaussian fit.

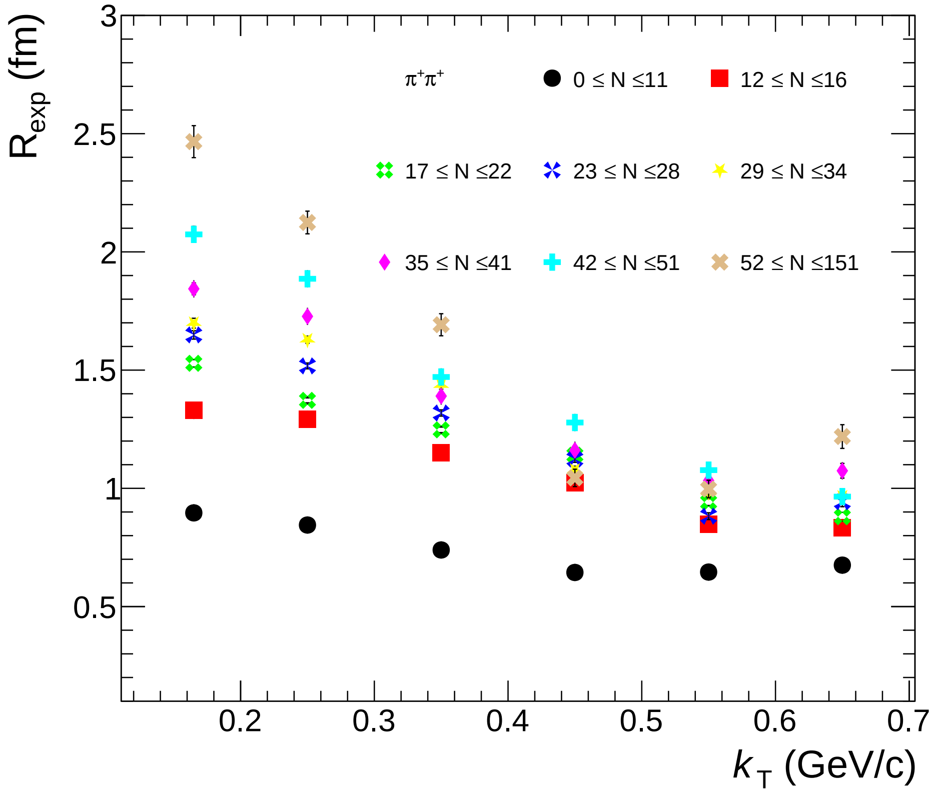

Figure 4.19: Source size R calculated for positive pions for Run 3 data from exponential fit, divided by $\sqrt{\pi}$.

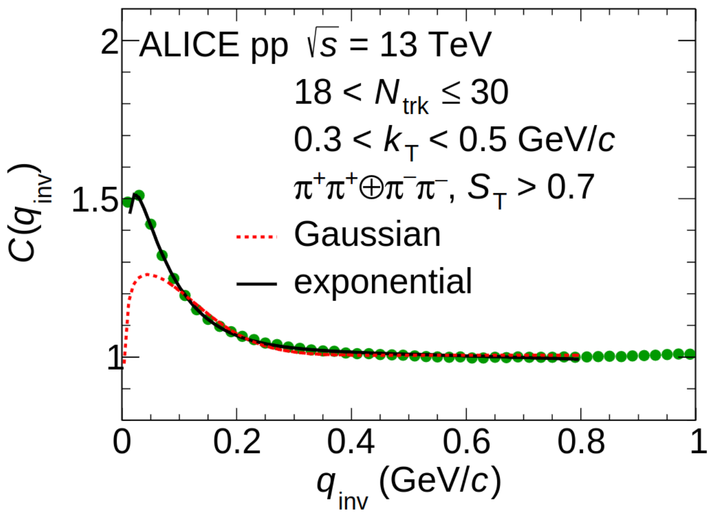

(Source: ALICE Collaboration. Femtoscopic correlations of identical charged pions and kaons in pp collisions at $\sqrt{s}$ = 13 TeV with event-shape selection, page 13. arXiv:2310.07509, 2023.)

Figure 4.20: Correlation function presented in ALICE Collaboration paper [5].

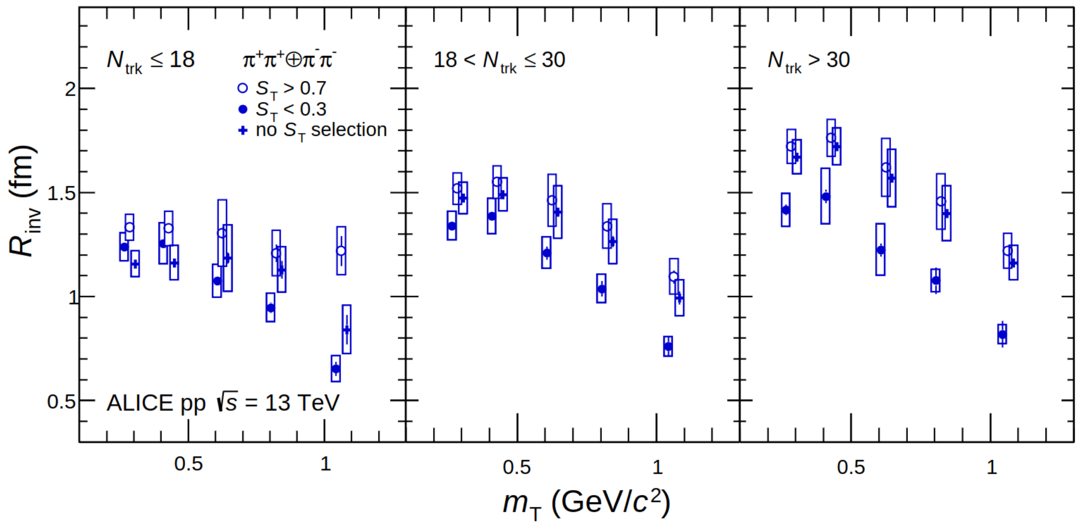

(Source: ALICE Collaboration. Femtoscopic correlations of identical charged pions and kaons in pp collisions at $\sqrt{s}$ = 13 TeV with event-shape selection, page 18. arXiv:2310.07509, 2023.)

Figure 4.21: Gaussian source size R_{inv} presented in ALICE Collaboration paper [5].

Chapter 5

Summary

In line with the aim of this thesis, I calculated femtoscopic correlations functions for pions in proton–proton collisions at energies of $\sqrt{s}$ = 13.6 TeV for data from LHC Run 3. With satisfactory statistics, I was able to carry out this analysis for different ranges of multiplicities and k_T. I also removed the background from these results using Monte Carlo datasets. Finally, by fit of calculated correlation function I obtained the source size R. The results presented are mostly in line with theoretical predictions, as well as with previously published results for pions. It was observed that the source size generally decreases with k_T and increases with multiplicity.

Another important part of this thesis was learning to use and developing the O^2 analysis framework requiring skills in $C++$ programming. In the future, this code can be further developed to allow more detailed analysis and make it more efficient.

The next step of presented analysis would be calculations of systematic uncertainty for correlation functions and source parameters. There is also potential for further development for instance by applying cut on sphericity to compare background removal methods. Another interesting point is the three–dimentional correlation analysis that is already being developed in the ALICE WUT group.

Bibliography

[1] O. Lock. The pion's pioneers. *CERN Courier Volume 27, Number 8, pp.11-17*, October 1987.

[2] R.L. Workman et al. (Particle Data Group). Prog. Theor. Exp. Phys. 2022, 083C01 (2022) and 2023 update.

[3] Ł. K. Graczykowski (Faculty of Physics, Warsaw University of Technology) for the ALICE Collaboration. What can we learn from femtoscopic and angular correlations of identified particles in ALICE? *EPJ Web of Conferences 172, 01007*, 2018.

[4] A. Riedel and G. Mantzaridis. PWGCF Hands-on session FemtoDream. *O2 Analysis Tutorial 2.0*, 27.04.2023.

[5] ALICE Collaboration. Femtoscopic correlations of identical charged pions and kaons in pp collisions at $\sqrt{s} = 13$ TeV with event-shape selection. *arXiv:2310.07509*, 2023.

[6] CERN website - About CERN. https://home.cern/about. Last accessed: 16.01.2024.

[7] CERN website - Our People. https://home.cern/about/who-we-are/our-people. Last accessed: 16.01.2024.

[8] CERN website - Our Mission. https://home.cern/about/who-we-are/our-mission. Last accessed: 16.01.2024.

[9] The ATLAS Collaboration. Observation of a new particle in the search for the Standard Model Higgs boson with the ATLAS detector at the LHC. *Phys.Lett.B 716 (2012) 1-29*, 2012.

[10] CERN website - Contribute to society. https://home.cern/about/what-we-do/our-impact. Last accessed: 16.01.2024.

[11] CERN website - Experiments. https://home.cern/science/experiments. Last accessed: 16.01.2024.

[12] CERN website - The Large Hadron Collider. https://home.cern/science/accelerators/large-hadron-collider. Last accessed: 16.01.2024.

[13] ALICE Collaboration K. Aamodt et al. The ALICE experiment at the CERN LHC. *JINST 3 S08002*, 2008.

[14] The ATLAS Collaboration et al. The ATLAS Experiment at the CERN Large Hadron Collider. *JINST 3 S08003*, 2008.

[15] The CMS Collaboration et al. The CMS experiment at the CERN LHC. *JINST 3 S08004*, 2008.

[16] LHCb Collaboration et al. The LHCb Detector at the LHC. *JINST 3 (2008) S08005*, 2008.

[17] ALICE website - Overview. https://alice.cern/overview. Last accessed: 16.01.2024.

[18] ALICE Collaboration website - ALICE Institutes. https://alice-collaboration.web.cern.ch/collaboration/alice_institute. Last accessed: 16.01.2024.

[19] ALICE Collaboration. ALICE upgrades during the LHC Long Shutdown 2. *arXiv:2302.01238*, 2023.

[20] M. Wolter (The Henryk Niewodniczański Institute of Nuclear Physics Polish Academy of Sciences). Metody analizy wielu zmiennych w fizyce wysokich energii. 2012.

[21] ALICE Collaboration. Particle identification in ALICE: a Bayesian approach. *arXiv:1602.01392*, 2016.

[22] H. Martins Silva et al for the ALICE Collaboration. The ALICE Glance Shift Accounting Management System (SAMS). *J. Phys.: Conf. Ser. 664 052037*, 2015.

[23] A. Alkin, G. Eulisse, J. Fiete, Grosse-Oetringhaus, P. Hristov, and M. Kabus. ALICE Run 3 Analysis Framework. *EPJ Web Conf. 251 (2021) 03063*, 2021.

[24] O2Physics code repository. https://github.com/AliceO2Group/O2Physics. Last accessed: 23.01.2024.

[25] ALICE O2 Analysis framework documentation. https://aliceo2group.github.io/analysis-framework/docs/gettingstarted/. Last accessed: 20.01.2024.

[26] CERN website - The Worldwide LHC Computing Grid (WLCG). https://www.home.cern/science/computing/grid. Last accessed: 01.01.2024.

[27] K. Aamodt et al. (ALICE Collaboration). Femtoscopy of pp collisions at $\sqrt{s} = 0.9$ and $\sqrt{s} = 7$ TeV at the LHC with two-pion Bose-Einstein correlations. *Phys. Rev. D 84, 112004*, 2011.

[28] Z. Chajęcki and M. Lisa. Global Conservation Laws and Femtoscopy of Small Systems. *Phys. Rev. C 78, 064903*, 2008.

[29] A. Kisiel (Faculty of Physics, Warsaw University of Technology). Program calculating Coulomb function. https://www.if.pw.edu.pl/~majanik/CERN/index.php/Femto. Last accessed: 13.01.2024.

List of Figures

List of Tables

Appendix A

Results for LHC22o_pass4_minBias_small and LHC23f4b2

As mentioned in sections 2.4 and 4.2 results for the second Run 3 p–p collisions at $\sqrt{s}$ = 13.6 TeV dataset LHC22o_pass4_minBias_small and anchored to it PYTHIA 8 dataset LHC23f4b2 are presented here due to their similarity with other analysed dataset.

Calculated purity and efficiency are shown in figure A.1. Similarly to results shown in figure 3.3 purity is high (95.73% for $\pi+$ and 95.72% for $\pi-$) and efficiency drops from over 60% to less than 30% when I start using TOF in particle identification.

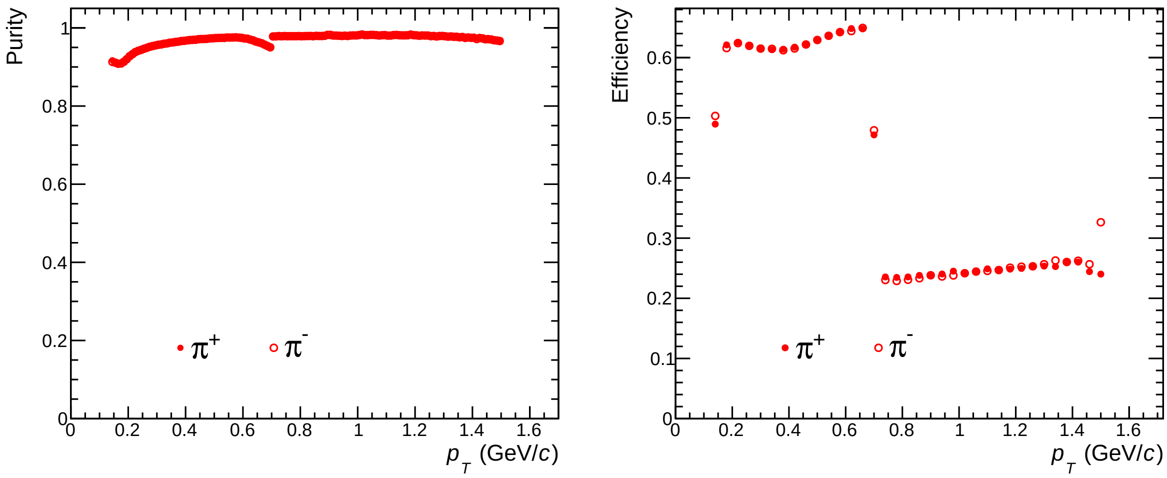

Figure A.1: Purity and efficiency for pions for PYTHIA 8 p–p collisions at $\sqrt{s}$ = 13.6 TeV simulation anchored to Run 3 (second dataset).

Histograms of n_σ for TPC and TOF are presented in figures A.2–A.5: A.2 and A.4 for Run 3 data, A.3 and A.5 for MC. dE/dx histograms are shown in figures A.6 and A.7. Conclusions that can be drawn from these figures are similar to those for the other dataset. dE/dx indicate good pions selection, as no other Bethe-Bloch curves are visible. n_σ between data and simulations are slightly shifted.

Figures A.8-A.13 shows QA histograms of pseudorapidity η, transverse momentum p_T and event multiplicity for both data and MC. Again for η and p_T differences between data and simulations can be spotted, larger than those observed for other dataset (in figures 3.16-3.19).

Figures A.14 and A.15 show numerators and denumerator of the pion correlation functions for Run 3 data and figures A.16 and A.17 show them for MC simulations. Calculated functions are shown in

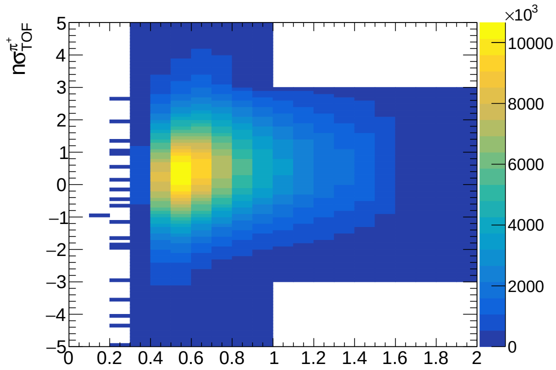

Figure A.2: n_{σ}^{TOF} for positive pions for p–p collisions at $\sqrt{s}$ = 13.6 TeV from Run 3 (second dataset).

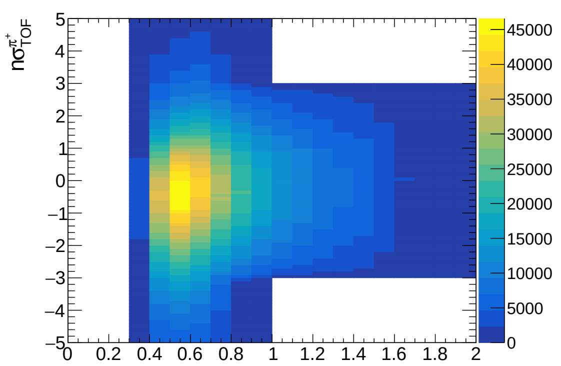

Figure A.3: n_{σ}^{TOF} for positive pions for PYTHIA 8 p–p collisions at $\sqrt{s}$ = 13.6 TeV simulation anchored to Run 3 (second dataset).

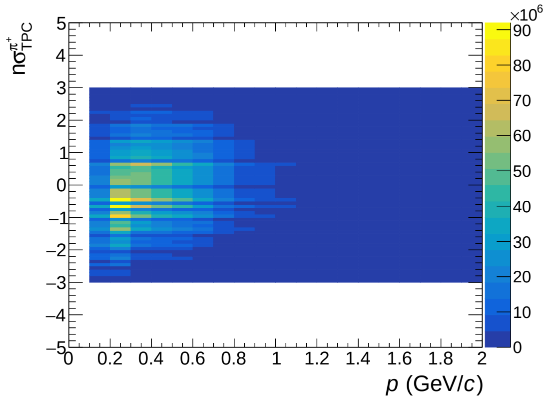

Figure A.4: n_{σ}^{TPC} for positive pions for p–p collisions at $\sqrt{s}$ = 13.6 TeV data from Run 3 (second dataset).

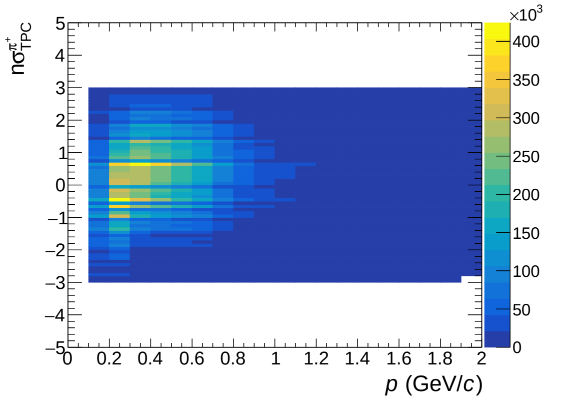

Figure A.5: n_{σ}^{TPC} for positive pions for PYTHIA 8 p–p collisions at $\sqrt{s}$ = 13.6 TeV simulation anchored to Run 3 (second dataset).

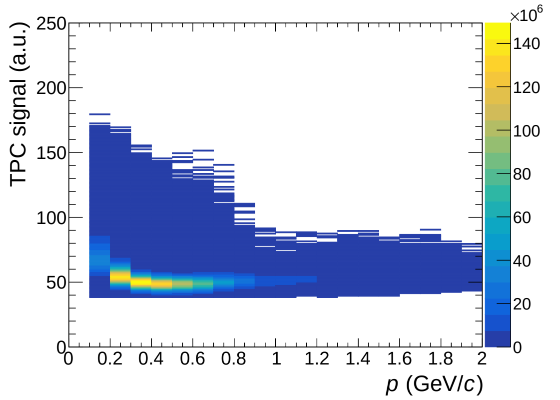

Figure A.6: dE/dx from TPC for positive pions for p–p collisions at $\sqrt{s}$ = 13.6 TeV data from Run 3 (second dataset).

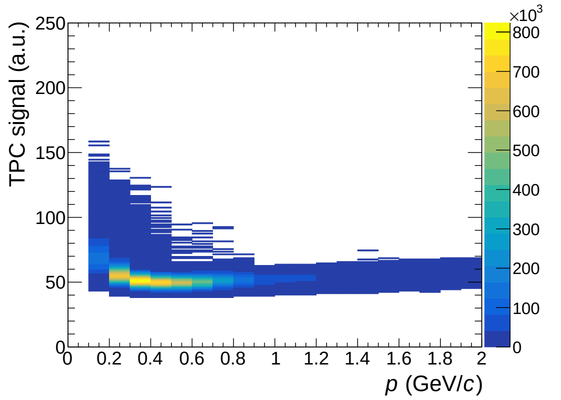

Figure A.7: dE/dx from TPC for positive pions for PYTHIA 8 p–p collsions at $\sqrt{s}$ = 13.6 TeV simulation anchored to Run 3 (second dataset).

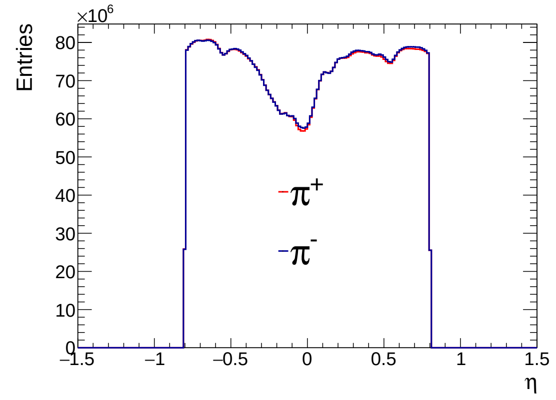

Figure A.8: η for pions for p–p collisions at $\sqrt{s}$ = 13.6 TeV data from Run 3 (second dataset).

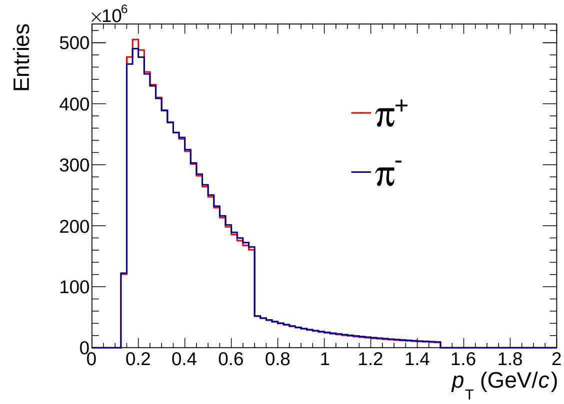

Figure A.9: p_T for pions for p–p collisions at $\sqrt{s}$ = 13.6 TeV data from Run 3 (second dataset).

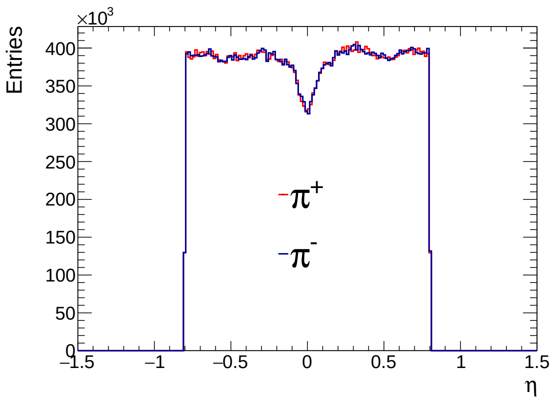

Figure A.10: η for pions for PYTHIA 8 p–p collsions at $\sqrt{s}$ = 13.6 TeV simulation anchored to Run 3 (second dataset).

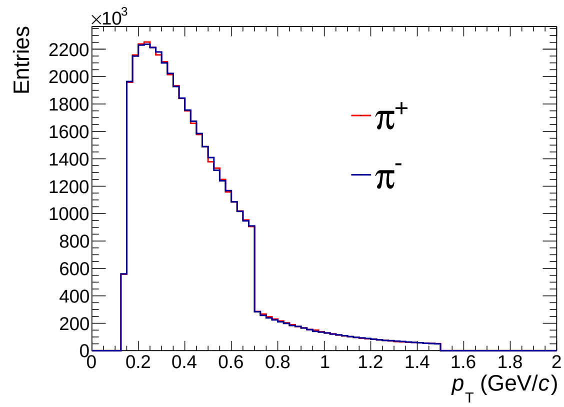

Figure A.11: p_T for pions for PYTHIA 8 p–p collsions at $\sqrt{s}$ = 13.6 TeV simulation anchored to Run 3 (second dataset).

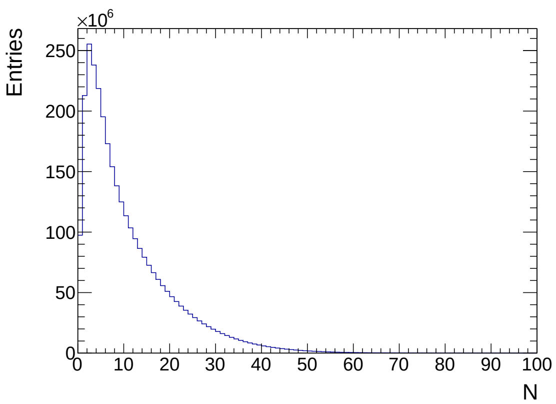

Figure A.12: Multiplicity of events for p–p collisions at $\sqrt{s}$ = 13.6 TeV data from Run 3 (second dataset).

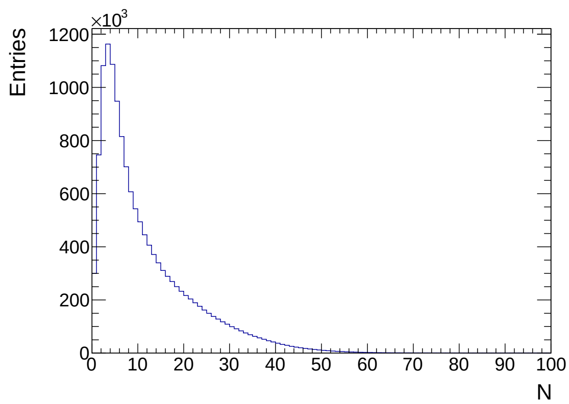

Figure A.13: Multiplicity of events for PYTHIA 8 p–p collisions at $\sqrt{s}$ = 13.6 TeV simulation anchored to Run 3 (second dataset).

figure A.18 and A.19. Figure A.20 shows results for MC simulations. They display same behaviour as functions presented before in figures 4.11 and 4.12. It can be observed that for data correlation function width increases with multiplicity and decreases with k_T. Statistics of MC dataset were not efficient for a proper fit and background removal, so I did not calculate source size R for those datasets.

Comparision between data and simulations is shown in figure A.21.

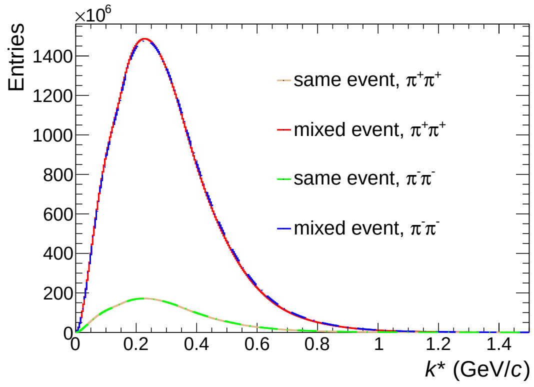

Figure A.14: k^* histogram for $\pi^+\pi^+$ and $\pi^-\pi^-$ for p–p collisions at $\sqrt{s}$ = 13.6 TeV data from Run 3 (second dataset).

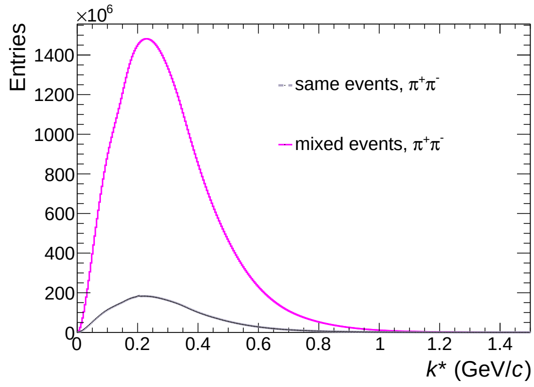

Figure A.15: k^* histogram for $\pi^+\pi^-$ pions for p–p collisions at $\sqrt{s}$ = 13.6 TeV data from Run 3 (second dataset).

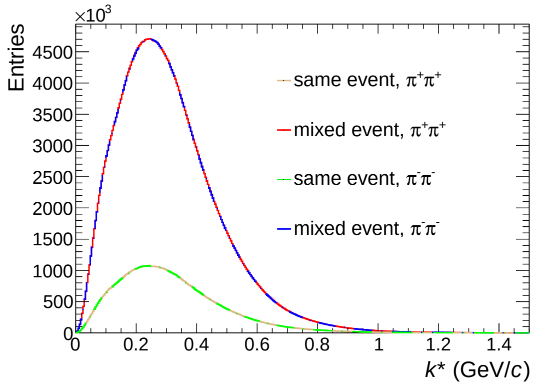

Figure A.16: k^* histogram for $\pi^+\pi^+$ and $\pi^-\pi^-$ pions for PYTHIA 8 p–p 13.6 TeV simulation anchored to Run 3 (second dataset).

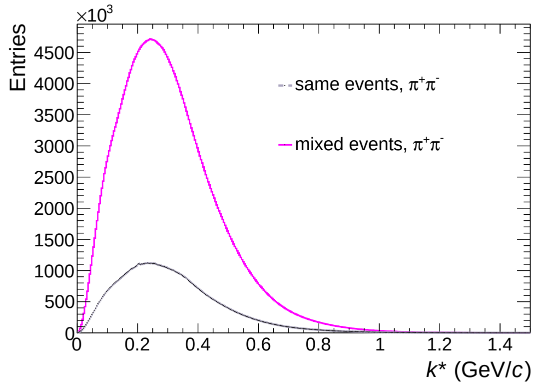

Figure A.17: k^* histogram for $\pi^+\pi^-$ pions for PYTHIA 8 p–p 13.6 TeV simulation anchored to Run 3 (second dataset).

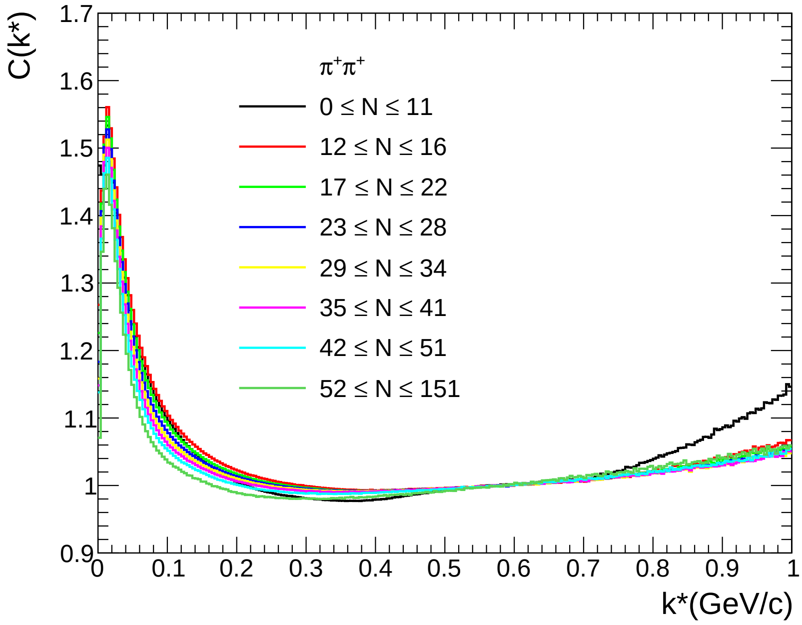

Figure A.18: Correlation functions for $\pi^+\pi^+$ for p–p collisions at $\sqrt{s}$ = 13.6 TeV data from Run 3 for different multiplicities ranges (second dataset).

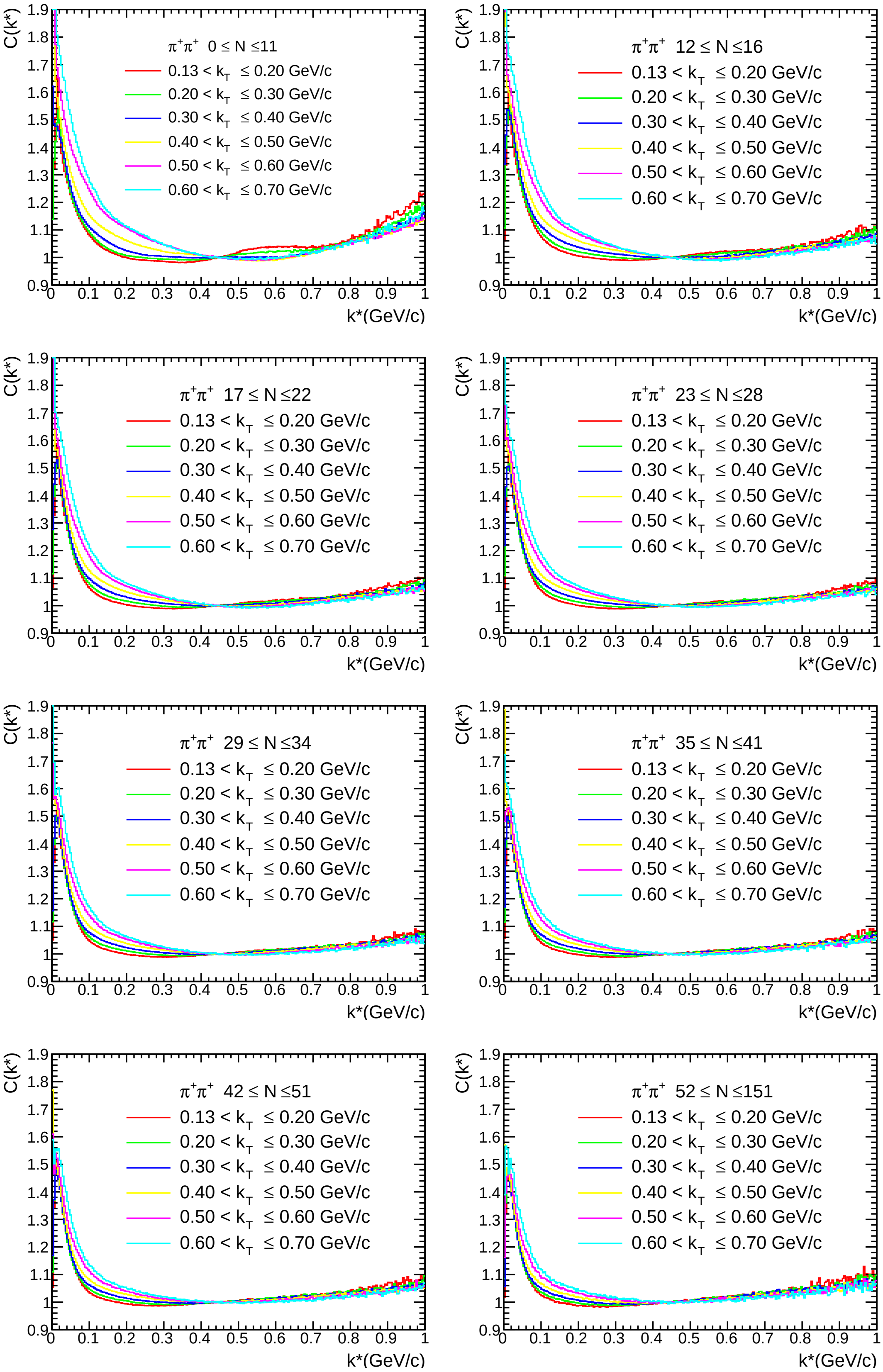

Figure A.19: Correlation functions for p–p collisions at $\sqrt{s}$ = 13.6 TeV data from Run 3 for different multiplicities and k_T ranges (second dataset).

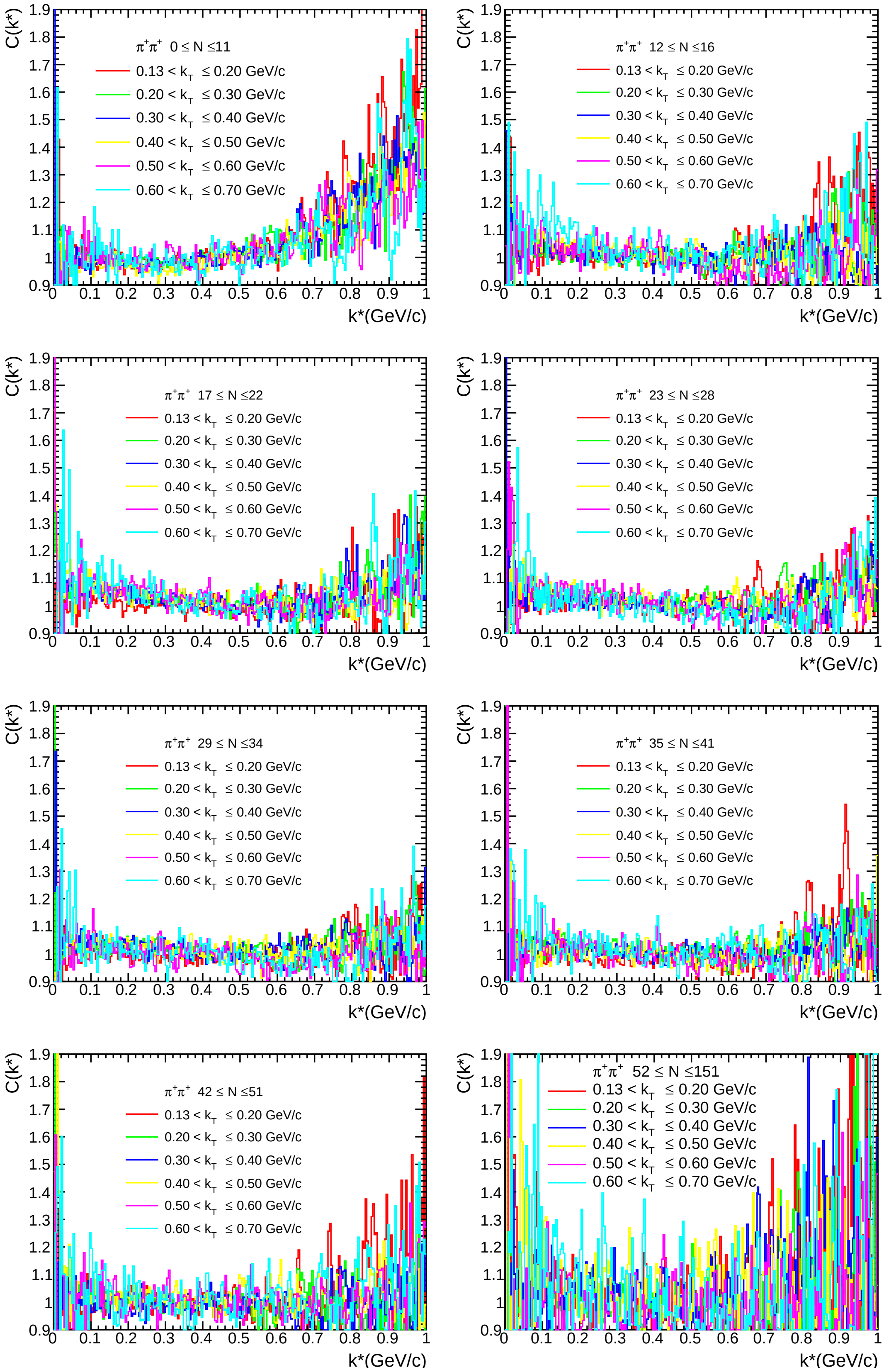

Figure A.20: Correlation functions for PYTHIA 8 p–p collisions at $\sqrt{s}$ = 13.6 TeV from Run 3 for different multiplicities and k_T ranges (second dataset).

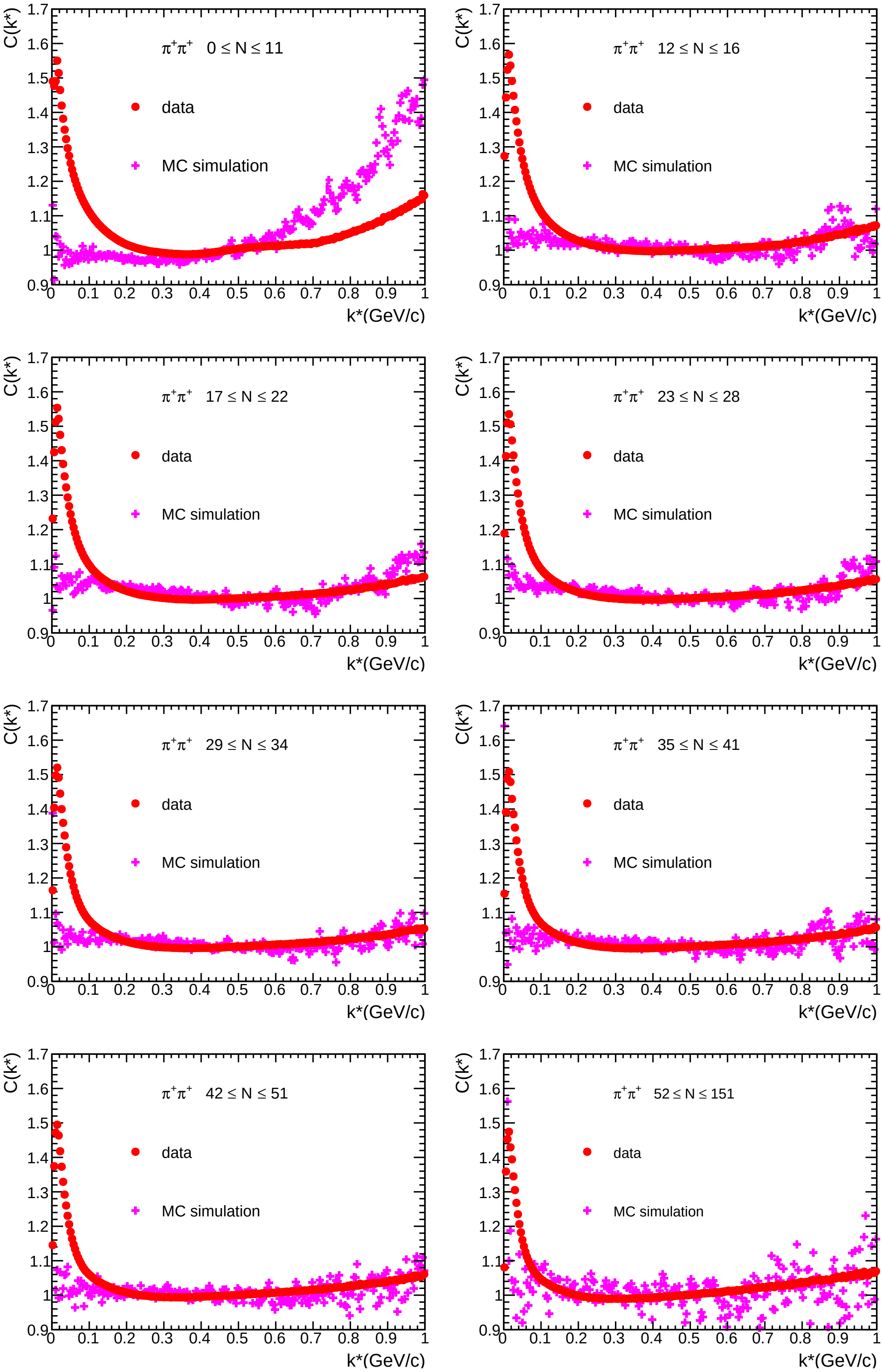

Figure A.21: Correlation functions comparison for p–p collisions at $\sqrt{s}$ = 13.6 TeV data from Run 3 and PYTHIA 8 p–p 13.6 TeV simulation anchored to Run 3 for positive pions (second datasets).